PHOTOPRODUCTION OF NEUTRAL PIONS FROM COMPLEX NUCLEI -- AN INDIRECT MEASUREMENT OF THE π^{o} LIFETIME

Thesis by

Henry Ruderman

In Partial Fulfillment of the Requirements

For the Degree of

Doctor of Philosophy

California Institute of Technology

Pasadena, California

1962

ACKNOWLEDGEMENTS

This experiment was suggested by Dr. A. V. Tollestrup who has supervised it throughout its course. Dr. R. Gomez has been a close collaborator since its inception. The association with them has proved to be extremely stimulating to the author during his graduate residency.

A large portion of the data was taken with the assistance of Mr. R. M. Talman who has provided several helpful suggestions. Some of the computer programs were coded with the help of Mr. W. Teitelman. The programs were run at the Western Data Processing Center under the aegis of Mr. W. P. Anderson.

Discussions on experimental questions with Drs. M. Sands and R. L. Walker and of a theoretical nature with Drs. S. M. Berman, C. A. Engelbrecht, M. Gell-Mann, H. Weidenmuller and F. Zachariasen have been greatly appreciated.

Much of the mechanical design was performed by Mr. B. H. Rule and Mr. D. Sell. The work of Mr. L. Loucks and his crew and of Mr. A. Neubieser and the machine operators is greatfully acknowledged. The experiment was run simultaneously with those of J. Chang, M. D. Daybell, and J. Kilner who were of assistance in various capacities. Discussions with Mr. C. Peck have also proven fruitful.

The partial financial support of the Dow Chemical Corporation has been greatly appreciated. The interest and encouragement of Dr. R. F. Bacher has been of much value.

ABSTRACT

The cross section for the photoproduction of neutral pions from complex nuclei at small angles has been measured in an attempt to determine the π^o lifetime from the reaction $\gamma + \gamma \rightarrow \pi^o$ where one of the photons is provided by the Coulomb field of the nucleus. Data were taken at energies near 950 Mev using targets of lead, copper, aluminum, carbon and oxygen. Both of the decay gamma rays from the pions were detected in total absorption counters so that an angular distribution of the pions could be calculated from the detector geometry and the partition of energy between the two counters. The cross section appears to be dominated by production from the individual nucleons adding coherently, leaving the nucleus in its ground state. The effects from the Coulomb production at the smallest angles allow us to exclude lifetimes shorter than 2×10^{-17} sec and longer than 1.5×10^{-16} sec. Because there is the possibility of systematic effects we quote the best value for the lifetime with large errors as $7.6 \, ^{+6.0}_{-4.5} \times 10^{-17}$ sec. The large coherent nuclear production indicates that the non-spin flip part of the nucleon cross section is peaked at small angles. If this is attributed to a pole in the scattering amplitude due to the exchange of a neutral vector meson, then the meson must be an isoscalar. We cannot distinguish between contributions from the mass 550 Mev and the mass 780 Mev particles.

TABLE OF CONTENTS

I. INTRODUCTION

Primakoff (1) has pointed out that there is a term in the photoproduction cross section for neutral pions from complex nuclei due to the same interaction that causes the decay of the π^o. This term comes from the incident photon interacting with a virtual photon in the Coulomb field and producing a pion, which is just the inverse of the decay process

$$\pi^o \rightarrow \gamma + \gamma \,. \qquad (1)$$

The differential cross section for the Coulomb production is strongly peaked at small angles and is proportional to the square of the nuclear charge and inversely proportional to the lifetime.

This experiment is an attempt to measure the production from the Coulomb field and, from the magnitude of the cross section, determine the π^o lifetime. The cross section is measured by detecting both of the γ-rays from the pion decay in energy sensitive Cerenkov counters. From the angular and energy distribution of the decay γ-rays, the angular dependence of the π^o cross section can be determined. Data have been taken at energies centered about 950 Mev from targets of lead, copper, aluminum, oxygen, and carbon.

Due to its characteristic angular distribution, the Coulomb production cross section can be disentangled from the other processes that produce neutral pions at small angles. These latter include coherent production in which the amplitudes from the individual nucleons add, interference between the Coulomb and coherent nuclear terms, and incoherent production leaving the nucleus in an excited state. The nuclear

processes give information about the cross sections from neutrons and protons in the forward direction. Several models for the nuclear production terms, including the possibility of having a pole in the amplitude due to a vector meson, have been considered.

The technique just described has been used by Davidson and Osborne (2) at 250 Mev who place a lower limit of 5×10^{-18} sec on the lifetime. The present experiment is an improvement over the one of Davidson and Osborne as it has been run at a higher production energy and with better angular resolution.

The π^o lifetime has been measured recently by several groups using a more direct method. These experiments involve measuring the distance between the point at which the pion is produced and the point at which it decays in a photographic emulsion. The latter point may be determined in the 1.2 percent of the decays in which a Dalitz pair is produced:

$$\pi^o \rightarrow e^+ + e^- + \gamma \,. \qquad (2)$$

The results of looking at monoenergetic neutral pions from $K^+ \rightarrow \pi^+ + \pi^0$ using stopped K mesons give lifetimes of $(3.2 \pm 1) \times 10^{-16}$ sec (3) and $(1.9 \pm 0.5) \times 10^{-16}$ sec (4). A mean life for the π^o of $(2.0\ ^{+0.5}_{-0.3}) \times 10^{-16}$ sec was determined from stars produced by high energy π^- mesons interacting in an emulsion (5). The difficulty that the neutral pi momentum spectrum had to be inferred from the charged pion spectrum is offset by the large time dilation factor.

The theoretical background for this experiment is discussed in

Section II. Section III contains a brief description of the experimental equipment used. A more complete description of the equipment and the procedure for data taking and analysis may be found in the appendices. Section IV presents the data, the backgrounds, the separation of the different contributions to the cross section, and the results. The conclusions are presented in Section V and suggestions are made for improvement of the experiment.

II. THEORETICAL BACKGROUND

A. Coulomb Production

The relationship between the total cross section for photoproducing neutral pions from a Coulomb field and the π^o lifetime was originally predicted by Primakoff (1). The differential cross section was calculated by Berman (6) from the diagrams in figure 1. In the production diagram 1a, a photon of four momentum k interacts with a virtual photon of momentum q in the Coulomb field of a spin zero nucleus of charge Ze producing a π^o of momentum p at an angle θ. The recoil energy of the nucleus is negligible so that the pion has essentially all the energy of the incident photon. At small momentum transfers in the forward direction the strength of the $\pi^o\gamma\gamma$ interaction is characterized by the π^o lifetime, as the same vertex appears in the diagram for the decay process 1b. The cross section for small q^2 is given by ($\hbar = c = 1$)

$$\frac{d\sigma_c}{d\Omega} = \frac{8Z^2\alpha}{m^3\tau} F_c^2(q)^2 \frac{p^3 k \sin^2\theta}{q^4} \tag{3}$$

$$q^2 = (k - p)^2 = E_\pi^2(1 + \beta^2 - 2\beta\cos\theta) \tag{4}$$

where $F_c(q^2)$ is the electromagnetic form factor of the nucleus as measured in electron scattering experiments and α is the fine structure constant.

As shown in figure 2, the Coulomb production at high energies is concentrated in a narrow angular region about the forward direction.

FIGURE 1

a PRODUCTION

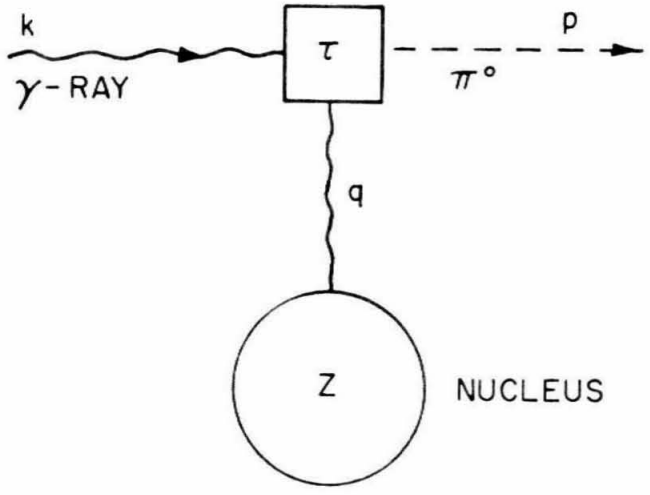

b DECAY

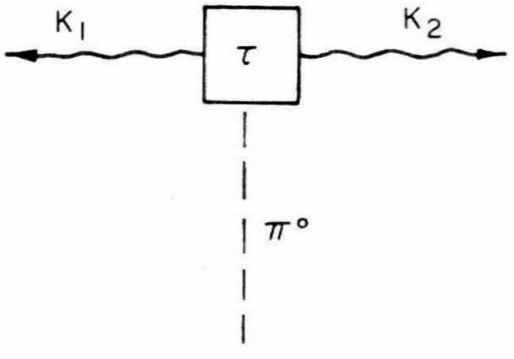

DIAGRAMS FOR COULOMB CROSS SECTION

Figure 2. Neutral pion photoproduction cross sections from lead at 900 Mev assuming no absorption. The parameters used are $\tau_{\pi^o} = 10^{-16}$ sec, $\sigma_{nsf} = 5 \sin^2\theta \mu b/sr$, and $\sigma_H = 1\ \mu b/sr$. The form factors are Gaussian as discussed in the text. For the incoherent term a correlation length $d = 1.5\ r_o$ was used.

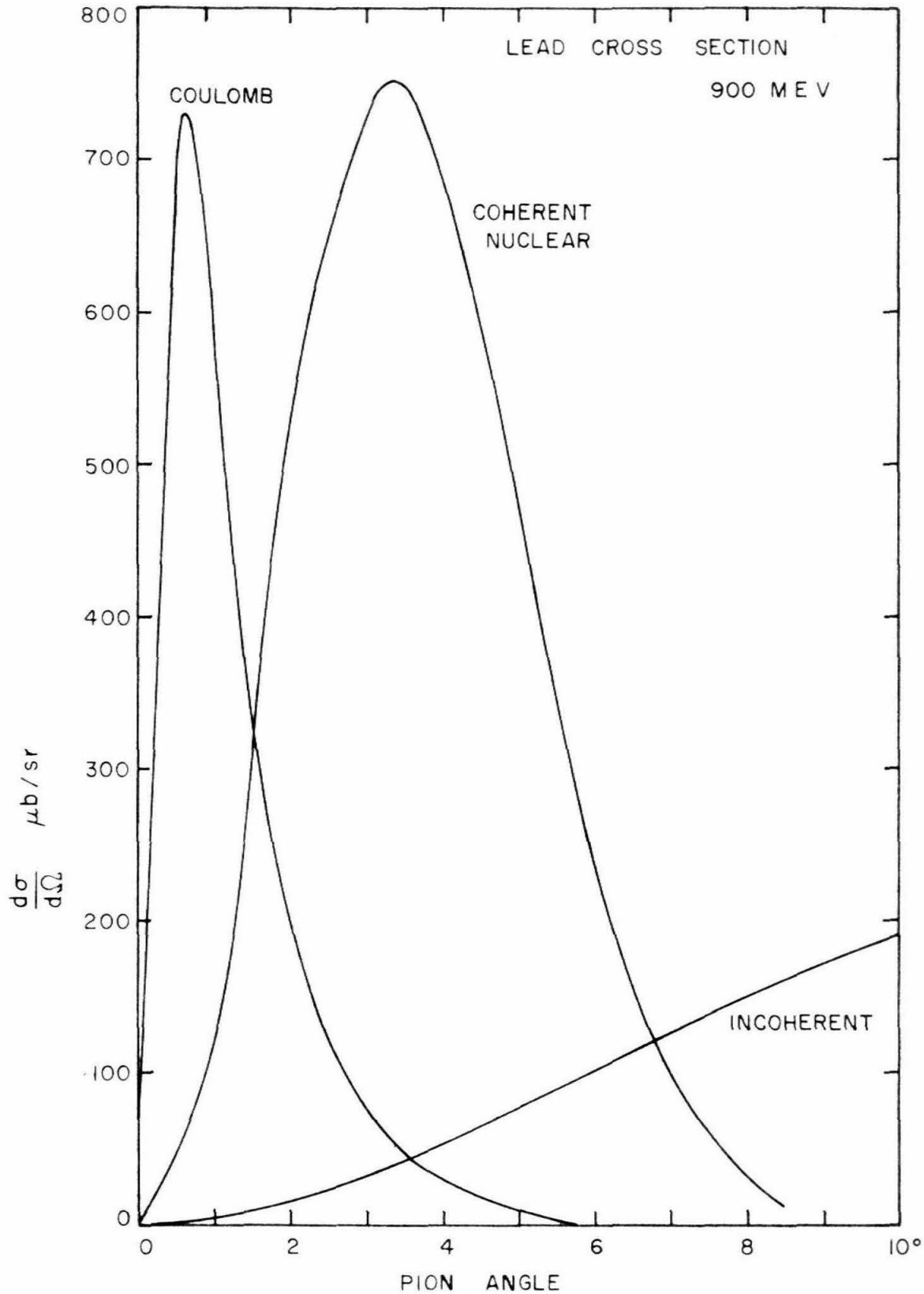
LEAD CROSS SECTION
900 MEV
COULOMB
COHERENT
NUCLEAR
INCOHERENT
800
700
600
500
400
300
200
100
0
0
2
4
6
8
10°
PION ANGLE
dσ/dΩ μb/sr

The maximum in the angular distribution occurs near $\theta = 1/2(m/k)^2$ and increases with the fourth power of the photon energy. If we take the form factor to be unity, then the total cross section is

$$\sigma_c = \frac{8\pi Z^2 \alpha}{m^3 \tau} \left[(1 + \beta^2) \ln \left(\frac{1 + \beta}{1 - \beta} \right) - 2\beta \right] \qquad (5)$$

which increases logarithmically with photon energy as shown in figure 3.

Since the pions produced in the Coulomb field can be considered in a crude way to have been made outside the nucleus, their final state interactions should be small. The absorption of those produced inside the nucleus has essentially the effect of increasing the root-mean-square radius or narrowing the diffraction pattern. This holds true for the more detailed calculation described in Part C of this section.

B. Nuclear Production

The photoproduction cross sections for neutral pions from complex nuclei has been calculated by Berman (7) and by Engelbrecht (8). For small momentum transfers and by use of the impulse and closure approximations, one can relate the nuclear cross sections to the elementary cross sections from free protons and neutrons. Since the elementary cross sections are not well known we will assume that the neutron and proton amplitudes are equal.

The nuclear cross section may be divided into coherent and incoherent parts. The coherent terms arise from those processes that leave the nucleus in its ground state, and are related to the non-spin

Figure 3. Total Coulomb cross section from lead as a function of energy for a π^o lifetime of 10^{-16} sec and unit form factor.

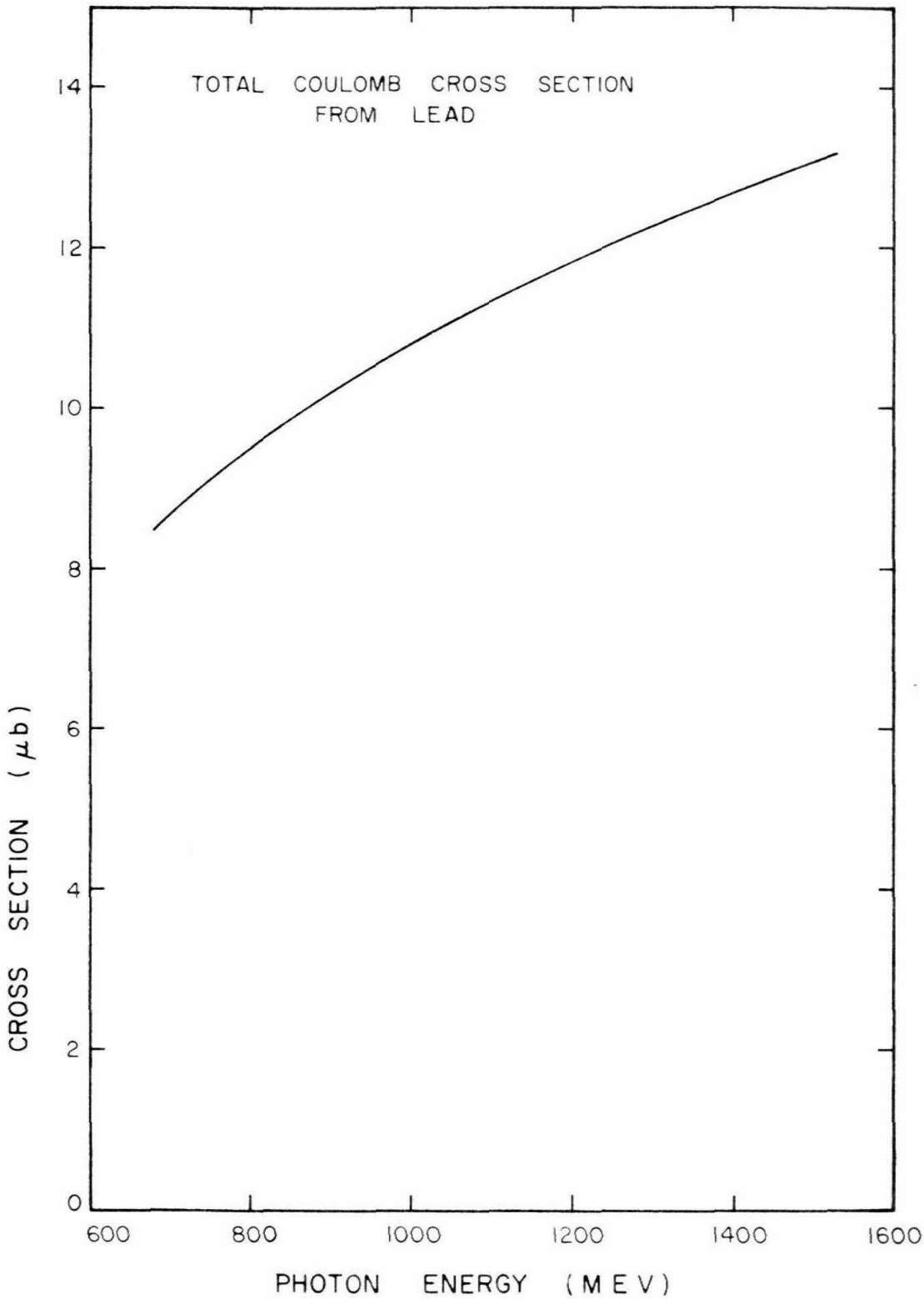
TOTAL COULOMB CROSS SECTION
FROM LEAD
CROSS SECTION (μb)
0
2
4
6
8
10
12
14
600
800
1000
1200
1400
1600
PHOTON ENERGY (MEV)

flip terms in the nucleon cross section. These all have a $\sin^2\theta$ dependence from the conservation of the longitudinal component of angular momentum so that the cross section goes to zero in the forward direction. Since all the nucleons contribute to the amplitude for these processes, the cross section in the limit of no final state absorption will be proportional to the square of the nucleon number (A^2). For convenience in comparing experimental data we write the coherent nuclear cross section in the form

$$\frac{d\sigma_n}{d\Omega} = A^2 \sin^2\theta \, F_n^2(q^2) \left[\frac{1}{\sin^2\theta} \frac{d\sigma_{nsf}}{d\Omega} \right] \tag{6}$$

where we have explicitly factored out the $\sin^2\theta$ dependence from the non-spin flip hydrogen cross section. The nuclear form factor $F_n(q^2)$ and the effects of final state interactions will be discussed below.

The incoherent terms arise when the nucleus is left in an excited state after the π^o has been emitted. We must then add the probabilities for each nucleon being excited giving a term proportional to the entire nucleon differential cross section and to A, again in the limit of no absorption. However, due to the exclusion principle, not all the states are available to an excited nucleon, especially at low momentum transfers. The factor $1 - G(q^2)$ with $G(0) = 1$ in the cross section represents this effect.

$$\frac{d\sigma_i}{d\Omega} = A\left[1 - G(q^2)\right] \frac{d\sigma}{d\Omega} \tag{7}$$

The suppression factor $1 - G(q^2)$ may be evaluated in terms of

the correlation length d introduced by Primakoff (9) in his analysis of muon capture in nuclei.

$$1 - G(q^2) = 1 - 3\mathcal{L}(qR)[1 - 1/2(d/r_o)^3(1 - \frac{2NZ}{A^2})] - \frac{3}{2}\mathcal{L}(qd)(d/r_o)^3(1 - \frac{2NZ}{A^2}) , \quad (8)$$

where

$$\mathcal{L}(x) = (\sin x - x \cos x)/x^3 ,$$

and $R = A^{1/3} r_o$ is the nuclear radius with $r_o = 1.25 \times 10^{-13}$ cm. We have used the value $d/r_o = 1.5$ as suggested by Primakoff.

Since the Coulomb and coherent nuclear pion production processes both leave the nucleus in the ground state these two interfere and produce an additional term in the cross section. Figure 2 shows the shapes of these cross sections for 900 Mev photons on a lead target, neglecting absorption.

C. Final State Interactions

In the limit of strong absorption only pions produced at the surface of the nucleus will be detected. Thus the A dependence of the nuclear cross sections would be $A^{4/3}$ for the coherent processes and $A^{2/3}$ for the incoherent. Engelbrecht (8) has further investigated the final state interaction using an optical model for the scattering and absorption of the pions in the nucleus. At 900 Mev he finds that only absorption is important. In general the angular distributions of the nuclear terms are only slightly affected except for a reduction in magnitude.

However, the first diffraction minimum in the Coulomb production moves towards smaller angles which also affects the interference term. In addition, the phase of the nuclear amplitude changes rapidly in the region of the peak in the cross section. These effects are illustrated in figures 4 and 5.

Engelbrecht has compared his absorption corrections to the coherent nuclear data taken at 250 Mev (2). The predicted nuclear cross section has the correct angular distribution but turns out a factor of four too small for calcium. Although the optical model should be better at higher energy, the poor agreement at low energy casts doubt on the validity of the whole calculation. This experiment shows the nuclear cross sections to be a factor of three larger than would be calculated by Engelbrecht using preliminary data from hydrogen. We are in the unfortunate situation that the uncertainties in the theory can cause systematic errors in the interpretation of the data. We can now neither predict the behavior of the nucleon cross section at small angles except in a qualitative way, nor can we use the measured hydrogen cross section to subtract the coherent nuclear contribution to our data to get a better value of the lifetime. We have decided to fit the data assuming the shapes are those without absorption using Gaussian form factors rather than those of Engelbrecht which depend on the details of a nuclear model. If the optical model predictions are correct, then we have overestimated the π^{o} lifetime and underestimated the nucleon cross section.

Figure 4. Effects of absorption on the Coulomb and coherent nuclear cross sections as calculated using an optical model. The parameters are the same as used in figure 2. The curves were constructed from the table on page 134 of Engelbrecht's thesis (8).

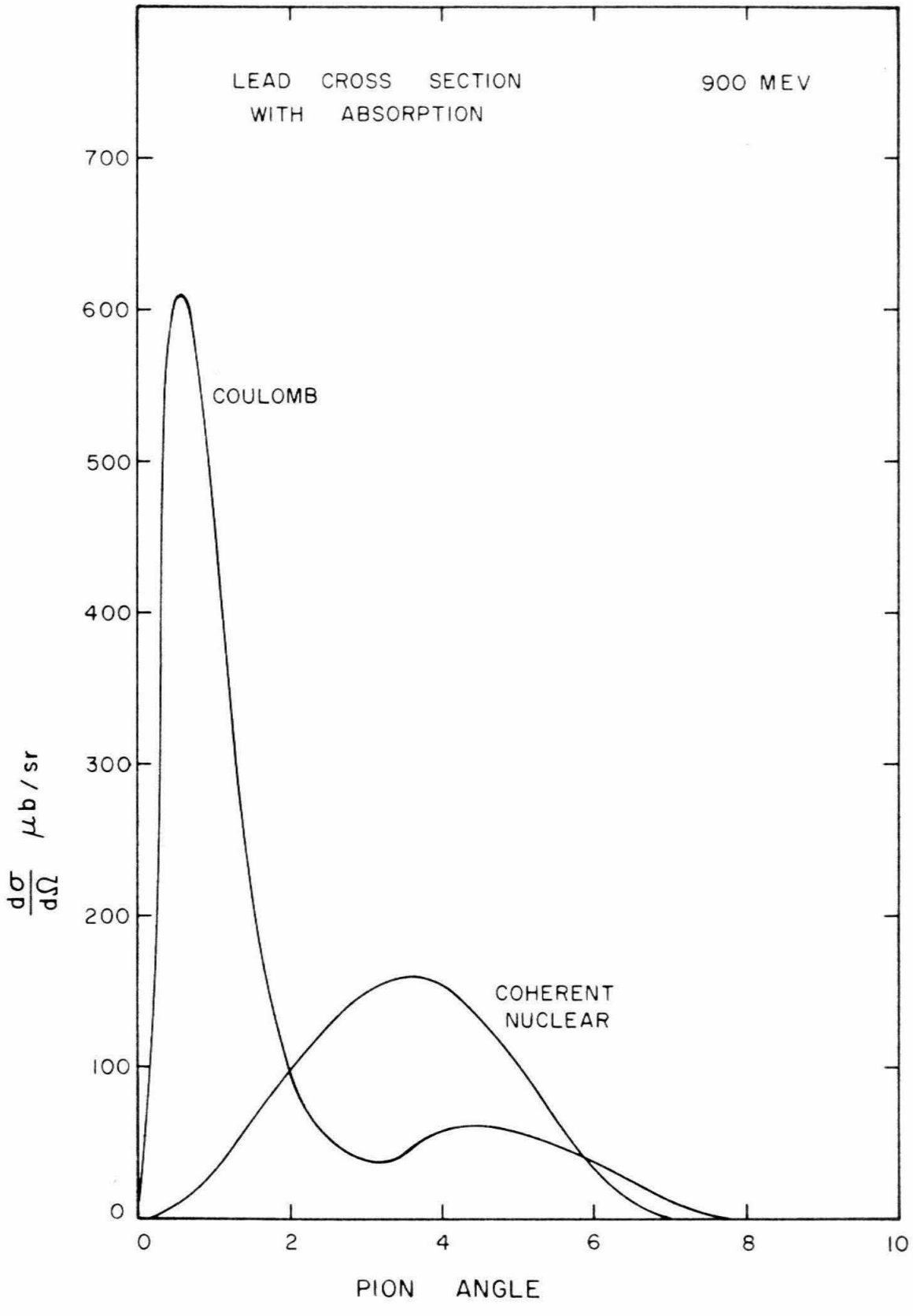
LEAD CROSS SECTION
WITH ABSORPTION
900 MEV
700
600
500
400
300
200
100
0
COULOMB
COHERENT
NUCLEAR
$\frac{d\sigma}{d\Omega}$ μb / sr
0
2
4
6
8
10
PION ANGLE

Figure 5. Effect of absorption on the cosine of the relative phase angle between the Coulomb and coherent nuclear amplitudes. The curve has been constructed from the table on page 134 of Engelbrecht's thesis (8).

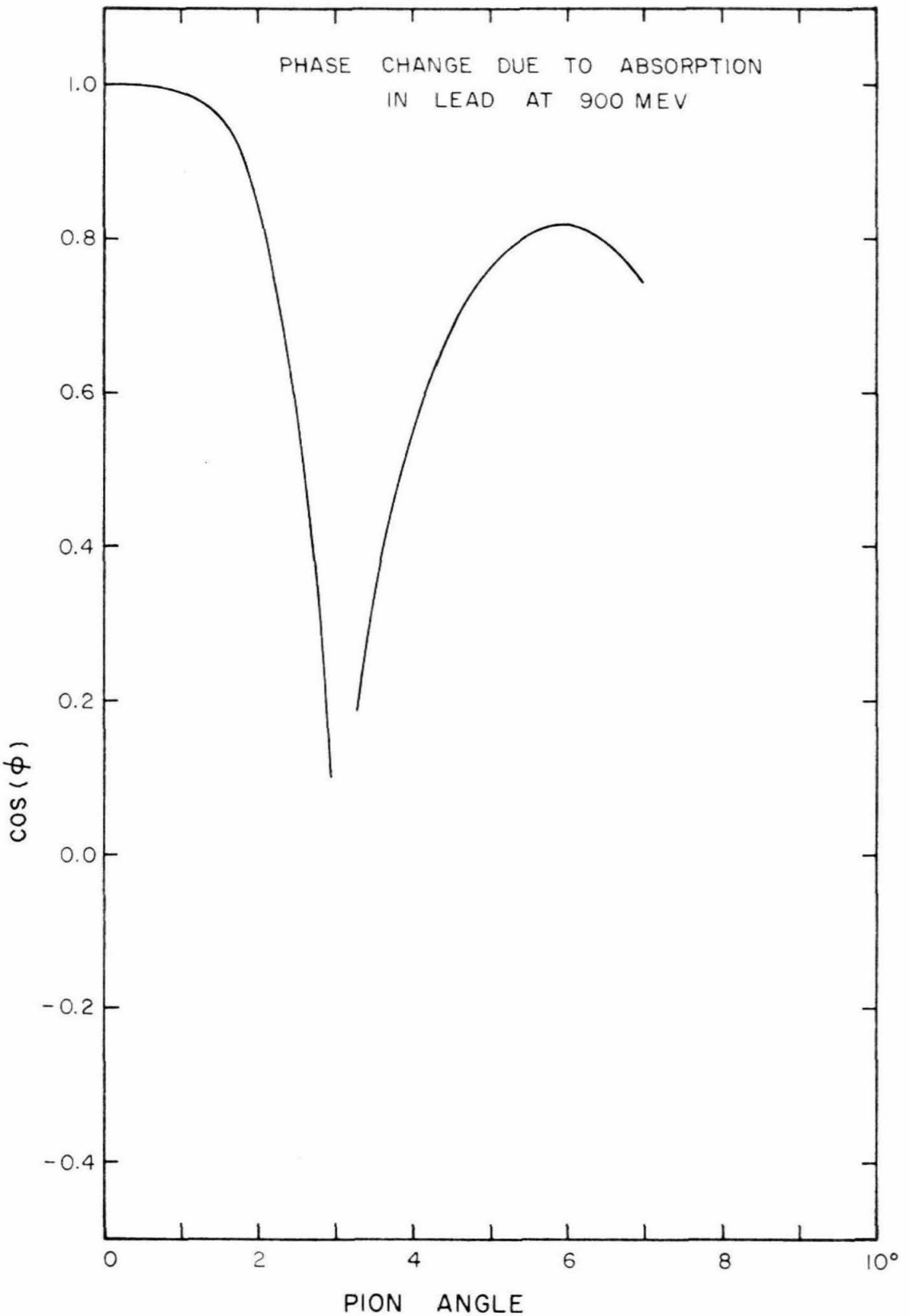
PHASE CHANGE DUE TO ABSORPTION
IN LEAD AT 900 MEV
1.0
0.8
0.6
0.4
0.2
0.0
-0.2
-0.4
COS (φ)
0
2
4
6
8
10°
PION ANGLE

III. EXPERIMENTAL TECHNIQUE

Both of the gamma rays from a neutral pion produced by the 1200 Mev bremsstrahlung beam in the target were detected in total absorption spectrometers. These Cerenkov counters (A and B) had a linear energy response to the incident photon. The angular acceptance was defined by lead apertures. By changing the angle δ between the beam direction and the plane through the target and the center lines of the apertures, an angular distribution was measured. The angle between the centers of the apertures was chosen to be the symmetric decay angle for a π^o with a total energy of 900 Mev. This energy is near the minimum between the second and third resonances in the total π^o photoproduction cross section. Charged particle events were eliminated by the sweeping magnet and by the veto counters (1A and 1B) covering the apertures. The cosmic ray veto counters (CR1 and CR2), located between the two Cerenkovs, served to reduce cosmic ray counts. The experimental arrangement is shown in plan view in figure 6.

A ten nanosecond coincidence between pulses from the Cerenkov counters is the initial identification of an event as a pion. If there were no pulses in any of the veto counters and the amplitudes of the Cerenkov pulses were sufficiently large, then these pulse heights were recorded on film for analysis. A block diagram of the electronic system is shown in figures 7 and 8. Details of the apparatus and electronics are discussed in Appendices A, B, and C. A description of the calibration and data handling procedures may be found in the appendices.

Figure 6. Plan view of experimental arrangement. The entire detector system is mounted on a table which moves in the vertical direction to measure an "angular distribution."

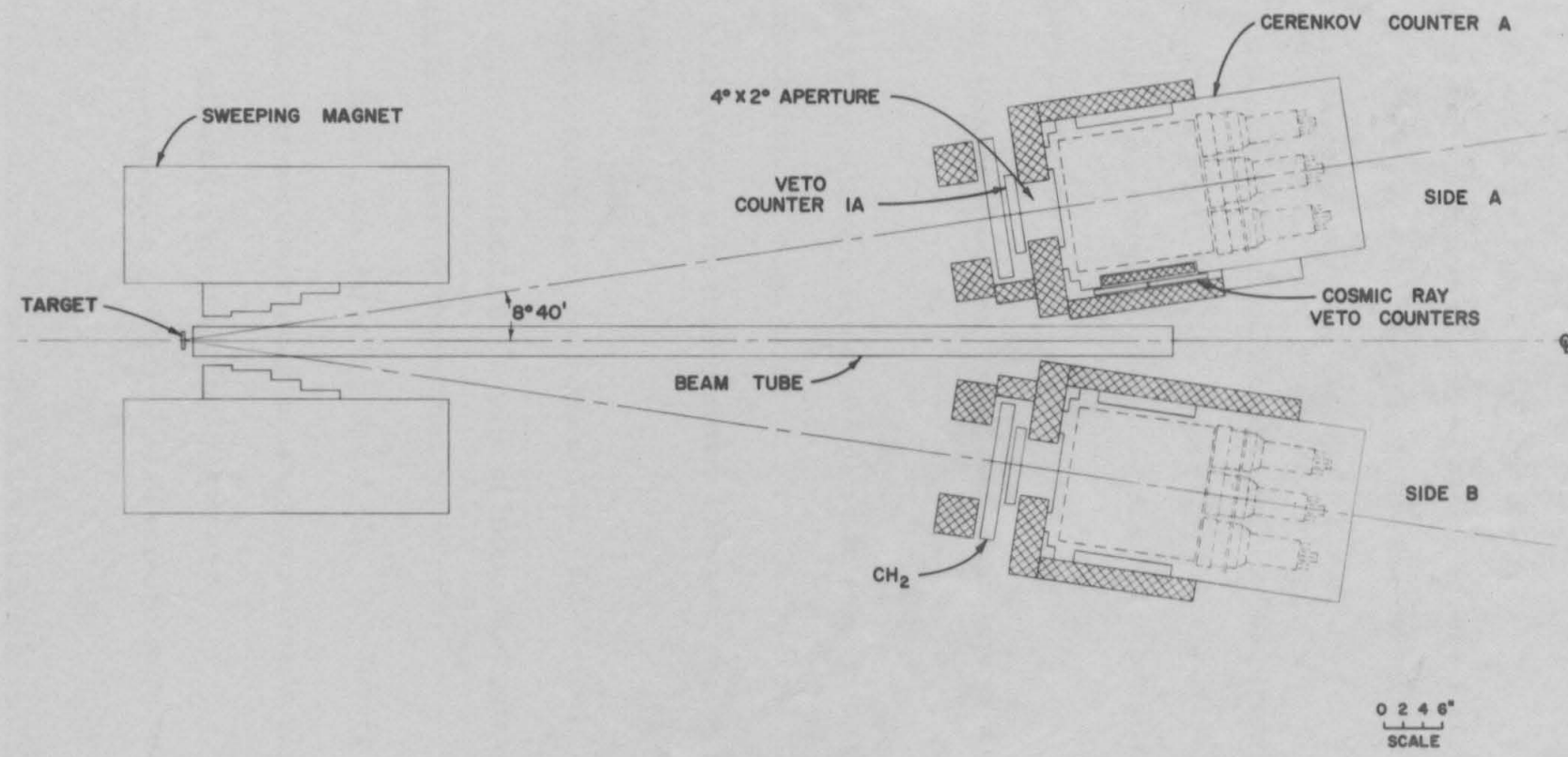

EXPERIMENTAL APPARATUS

Figure 7. Block Diagram of Fast Electronics.

All circuits are transistorized except for the distributed amplifiers. The figures in parentheses are the circuit drawing number. A brief description of the circuits follows.

MIXER: Adds nine input signals three at a time and then sums the triplets. Outputs for (123), (456), and (789) sums in addition to the 1-9 sum. Calibration input to the nine channels in parallel.

ATTN: Step attenuators.

HPA, HPB: Hewlett-Packard distributed amplifiers type 460A and 460B.

DELAY MIXER: Adding circuit with delay in each channel adjusted by external cables.

MULTI: Multiplexor with three emitter follower outputs for each input. (10-T-538)

F.C.: Fast coincidence circuit model 705. (10-T-468)

DOUBLE GATE AND ADDER: A pair of linear fast gates. The two gated signals are added at the output. (10-T-618)

AMP: Slow, fixed gain amplifier Model 721. (10-T-549)

STCH: Linear stretching circuit to lengthen pulses to 0.25 μsec. There is a calibration input on each stretcher.

The operation of the system is described in Appendix C.

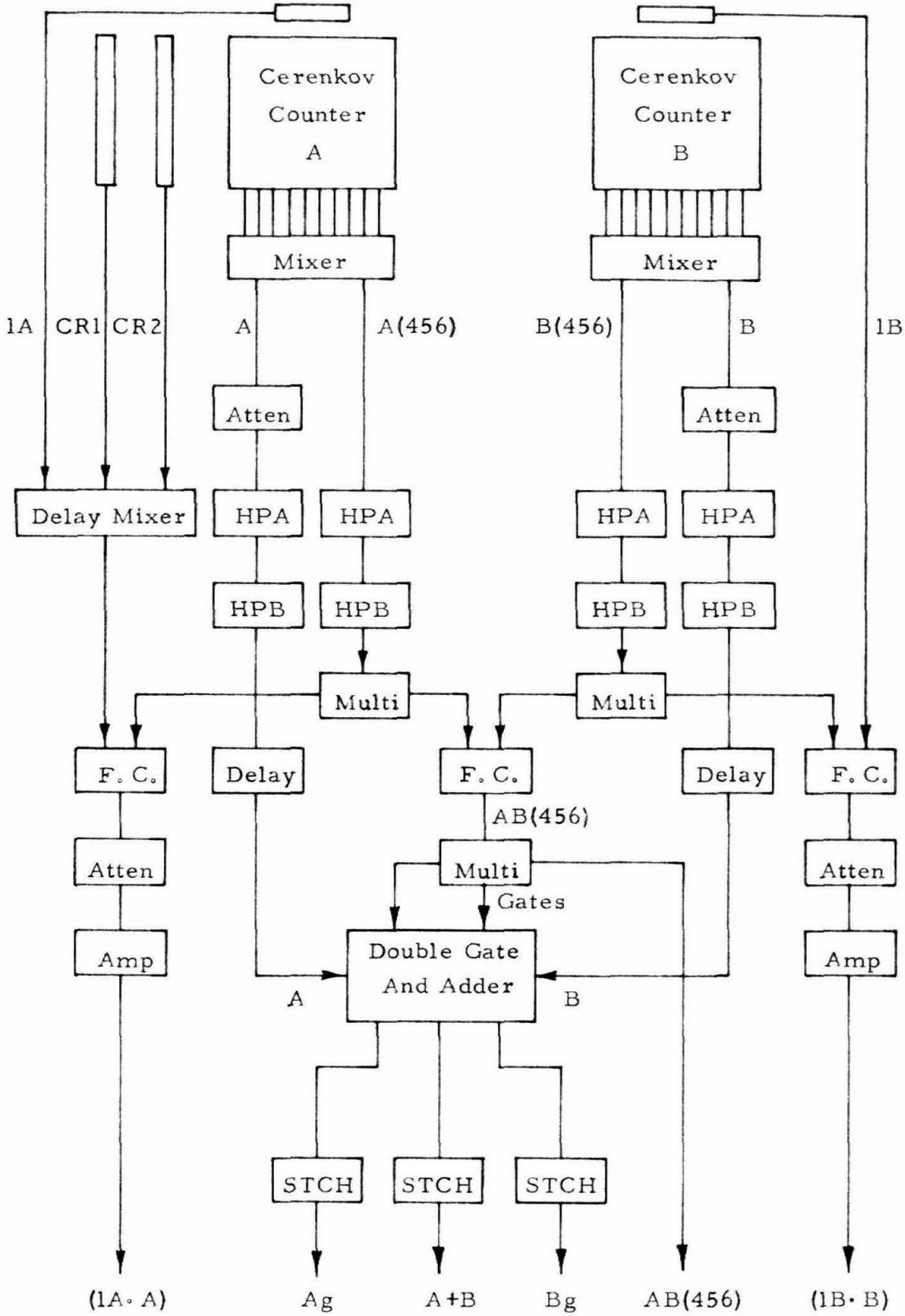

FAST ELECTRONICS BLOCK DIAGRAM

Figure 8. Block Diagram of Slow Electronics

A brief description of the circuits follows.

522A: 0.1 μsec. rise time, 0 - 2.5×10^3 gain amplifier.

KECK BOX: Six channel discriminator and coincidence-anti-coincidence circuit gated on during the beam dump.

SCAL: Decimal scaling units.

KICKSORTER: Twenty channel pulse height analyser.

DOUBLE GATED STRETCHER: Amplitude preserving pulse stretcher. Gives an output for oscilloscope unblanking.

SCOPE: Tektronix type 513D oscilloscope.

The operation of the system is described in Appendix C.

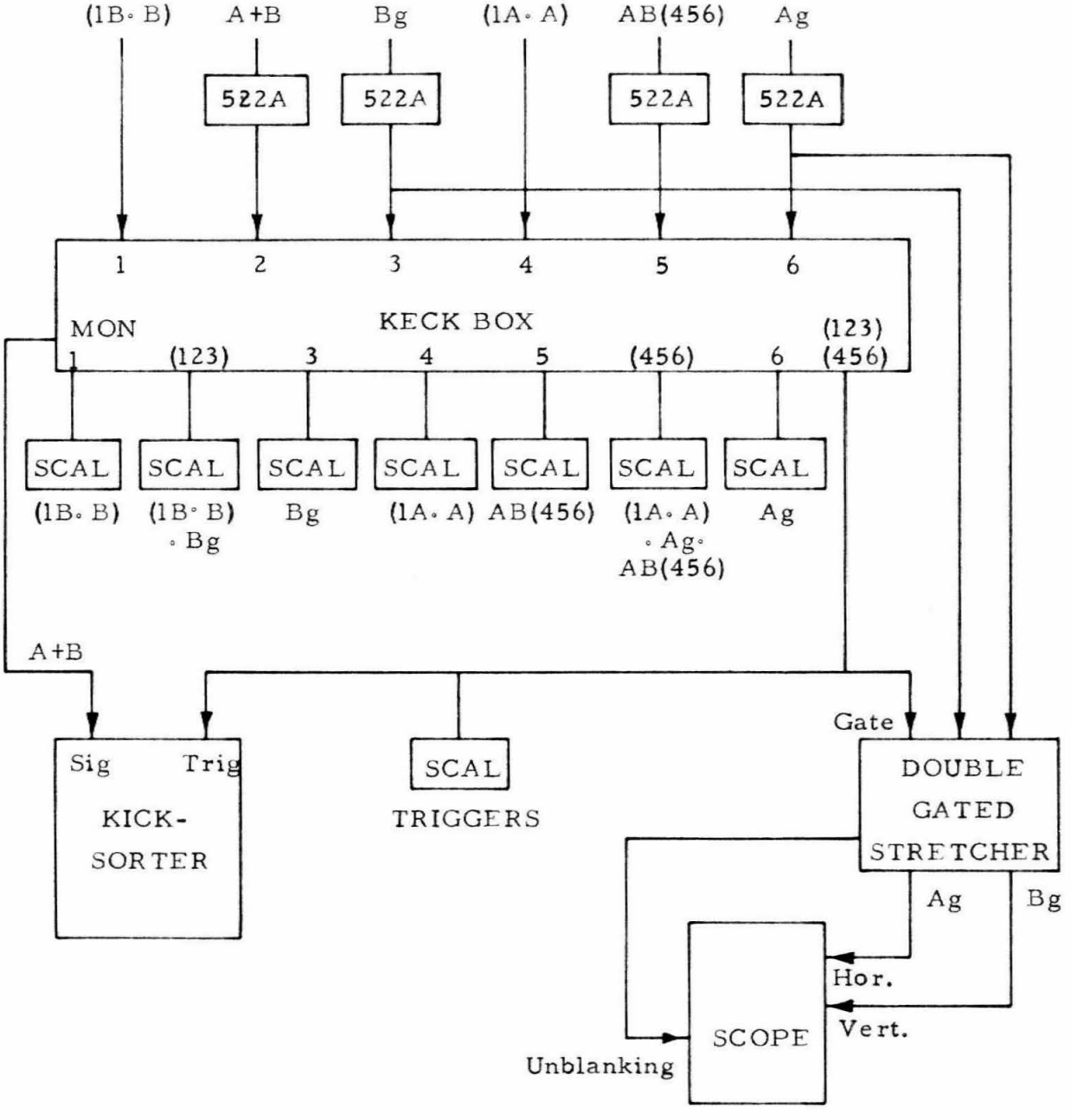

SLOW ELECTRONICS BLOCK DIAGRAM

IV. DATA AND RESULTS

A. Angle and Energy Distributions

The spectrum of the sum of the energies of coincident γ-rays has been plotted in figure 9. The peak in the spectrum near 950 Mev is a strong indication that they have come from π^o decays. The fall off of the counting rate toward high energies is due primarily to the shape of the bremsstrahlung spectrum; the fall off toward lower energies is due to a decrease in the effective solid angle of the detector system, reaching zero near 750 Mev where the minimum opening angle between the decay photons is greater than the maximum angular aperture. There is, however, especially at small angles, a low energy background. These events have been investigated and, although their source has not been fully understood, they appear to be due to processes in which the incident particle (a photon or possibly electrons produced in the air) initiates an electron-photon shower in the target. The counting rate for these events increases faster than linearly with target thickness. A second source may be photons from two different pions in multiple π^o production. The target thickness was chosen to be a compromise between background and foreground counting rates.

To minimize the contribution from these spurious counts only "pi like" events were used in analyzing the data. A "pi like" event had an energy division between the two counters consistent with that from the decay of a π^o produced in the target. Qualitatively, one can see that if the pion had energy lower than 900 Mev so that the minimum angle between

Figure 9. Energy spectrum of the sum of the pulse heights from both Cerenkov counters from the lead target at counter positions of 0.0° and 2.9°. The solid and broken histograms are the measured spectra for all events and for only "pi like" events respectively. The cut off near 400 Mev is due to an electronic bias. The solid curve is the spectrum predicted for coherent nuclear production alone by a Monte-Carlo integral with the energy response of the detectors folded in.

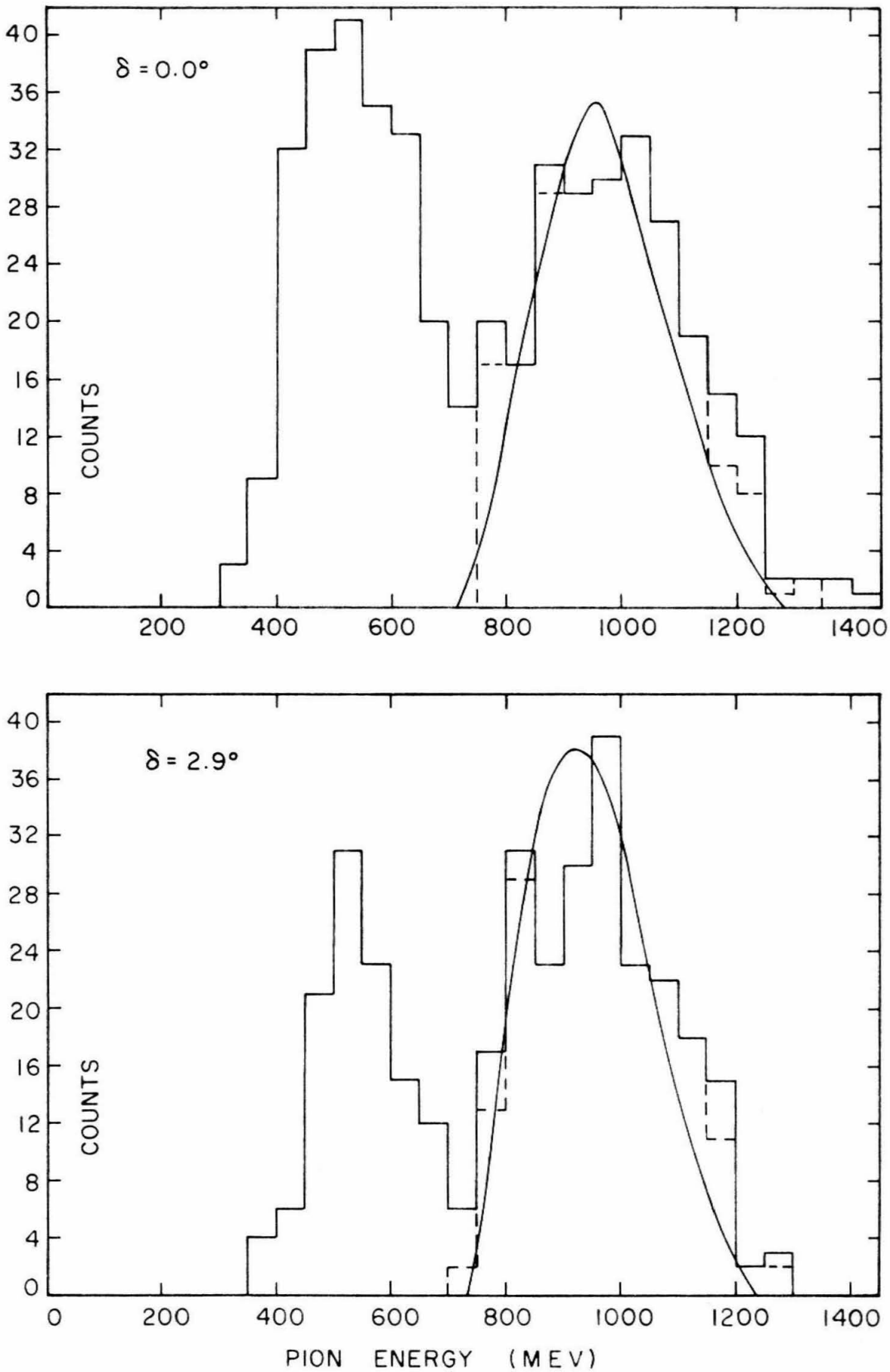
δ = 0.0°
δ = 2.9°
COUNTS
COUNTS
0
4
8
12
16
20
24
28
32
36
40
200
400
600
800
1000
1200
1400
PION ENERGY (MEV)

the two decay photons was greater than the mean opening angle between the two counters, then the total energy of the pion would be partitioned nearly equally. For a higher energy pion, where the minimum decay angle is less than the minimum angle between the apertures, it is impossible to detect an event in which the photon energies are equal. The method of calculating whether an event was "pi like" is described in Appendix E.

The counting rates as a function of counter position (δ) and the backgrounds are presented in Table I and plotted in figures 10 - 13. The data have been corrected for γ-ray absorption in the target and in the paraffin in front of the detectors. The counting rate as a function of pion angle has been calculated in the following manner. Let E_A and E_B be the measured energy of the photons detected by counters A and B, and let $E_\pi = E_A + E_B$ and $\epsilon = E_A - E_B$, then the angle between the pion and γ-ray directions is given by

$$\tan \theta_A = \frac{m_\pi(\beta^2 E_\pi^2 - \epsilon^2)^{1/2}}{E_\pi(\beta^2 E_\pi + \epsilon)}$$

$$\tan \theta_B = \frac{m_\pi(\beta^2 E_\pi^2 - \epsilon^2)^{1/2}}{E_\pi(\beta^2 E_\pi - \epsilon)} \quad .$$

From the angular limits on the apertures we can now calculate the maximum and minimum possible pion production angle, θ_{max} and θ_{min}, with respect to the center line between the counters. We then define the pion angle by

$$\theta_\pi = [\ \delta^2 + (\theta_{max} + \theta_{min})^2/4]^{1/2} \quad . \qquad (9)$$

To take into account the improved angular resolution achieved by calculating the pion angle, the data at small δ were lumped into one degree bins. The fitting of the theoretical counting rates was performed on this combination of δ and θ_π data.

The data in this form are hard to visualize, so that for presentation purposes only the data have been treated as follows. For each δ a histogram of counting rates for pion angles with one degree intervals was constructed. If we define $R(\delta_i, \theta_j)$ as the measured counting rate for "pi like" events with $\theta_j - 1/2^o \leq \theta_\pi \leq \theta_j + 1/2^o$ at counter position δ_i and similarly define $R_o(\delta_i, \theta_j)$ as the calculated counting rate for a constant cross section, then we form the normalized counting rate

$$N(\theta_j) = \frac{\Sigma_i R(\delta_i, \theta_j)}{\Sigma_i R_o(\delta_i, \theta_j)}$$

which is plotted in figures 14 - 17. By this calculation we have attempted to unfold the angular resolution of the detector system and to reconstruct the original cross section. The angular resolution has been cut down to about two degrees. It is difficult to treat the data in a statistically consistent way by this procedure as the counter resolution changes rapidly with counter position. The data as plotted in figures 14-17 have the error flags overestimated so that a goodness of fit test is not valid. The primary purpose is to show the shapes and magnitudes of the cross sections.

TABLE I

Counting Rates (counts/100 bips) Corrected for Absorption

Target Counter Position	Lead	Copper*	Aluminum	Carbon	Out	Oxygen	Thermos
0.0°	1.76 ± 0.12	2.83 ± 0.21	4.38 ± 0.34	3.81 ± 0.24	0.25 ± 0.08	10.97 ± 0.88	2.02 ± 0.21
1.0	1.44 ± 0.14	2.78 ± 0.21 (4.79 ± 0.77)			0.08 ± 0.05		
1.9	1.54 ± 0.13	2.89 ± 0.20	5.32 ± 0.64	4.65 ± 0.99	0.18 ± 0.08		
2.9	1.45 ± 0.10				0.14 ± 0.06		
3.8	1.13 ± 0.13	3.81 ± 0.26	6.33 ± 0.33	6.87 ± 0.38	0.16 ± 0.07		
4.8	0.87 ± 0.11				0.08 ± 0.05		
5.8	0.47 ± 0.06	3.18 ± 0.68 (4.11 ± 0.35)	6.10 ± 0.36	7.31 ± 0.58	0.13 ± 0.05	18.62 ± 1.19	2.88 ± 0.33
7.7	0.23 ± 0.05	1.64 ± 0.33 (2.88 ± 0.25)	3.66 ± 0.34	7.46 ± 0.61	0.04 ± 0.04		
10.5	0.22 ± 0.05	0.53 ± 0.08	1.98 ± 0.24	3.76 ± 0.31	0.08 ± 0.04		

*Copper data in parenthesis is from the 2.94 gm/cm^2 target. The rest of the copper data is from the 1.43 gm/cm^2 target.

Figures 10 - 13. Counting rates for "pi like" events as a function of counter position with backgrounds subtracted and corrected for photon absorption.

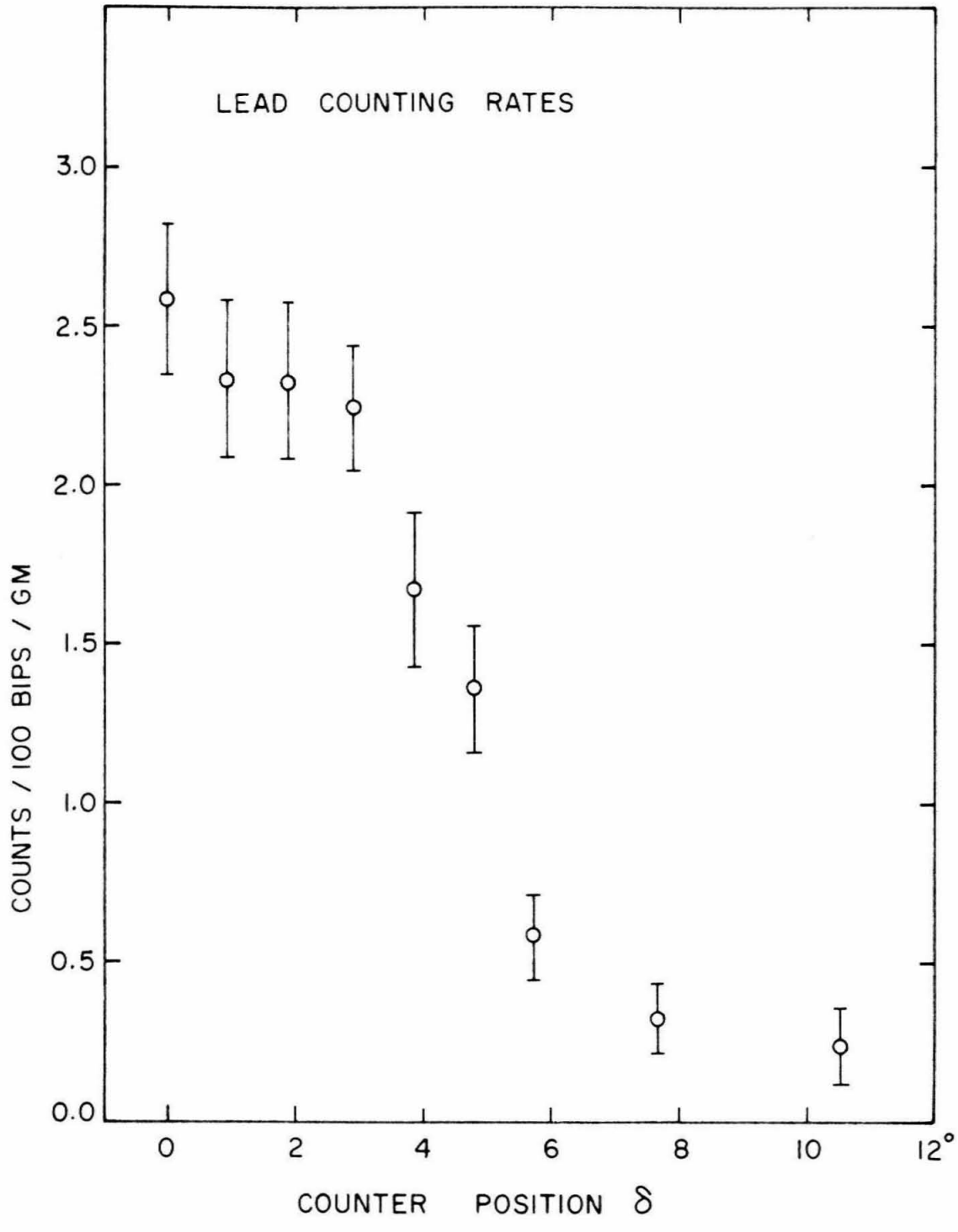
LEAD COUNTING RATES
COUNTS / 100 BIPS / GM
3.0
2.5
2.0
1.5
1.0
0.5
0.0
0
2
4
6
8
10
12°
COUNTER POSITION δ

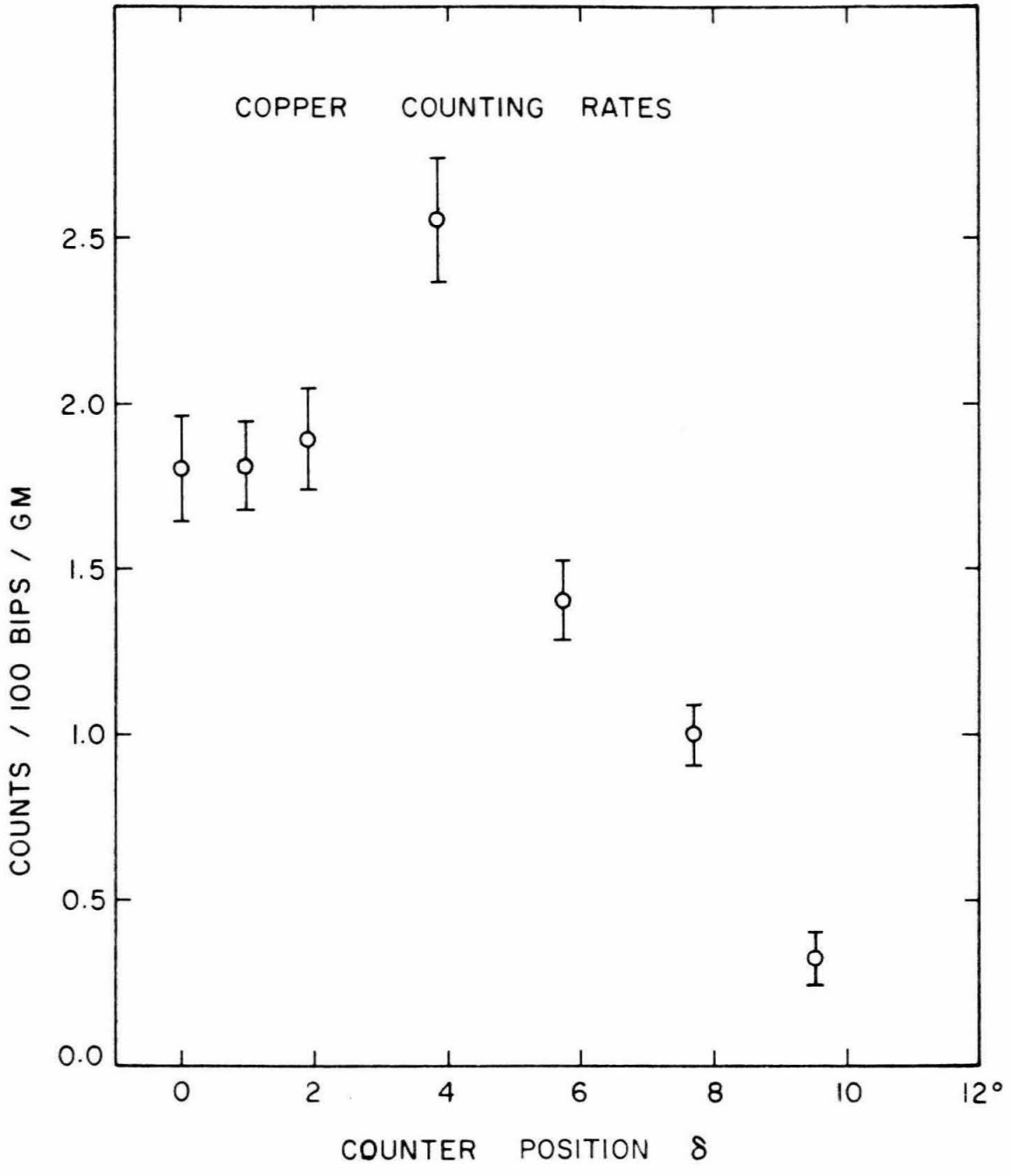
COPPER COUNTING RATES
COUNTS / 100 BIPS / GM
0.0
0.5
1.0
1.5
2.0
2.5
0
2
4
6
8
10
12°
COUNTER POSITION δ

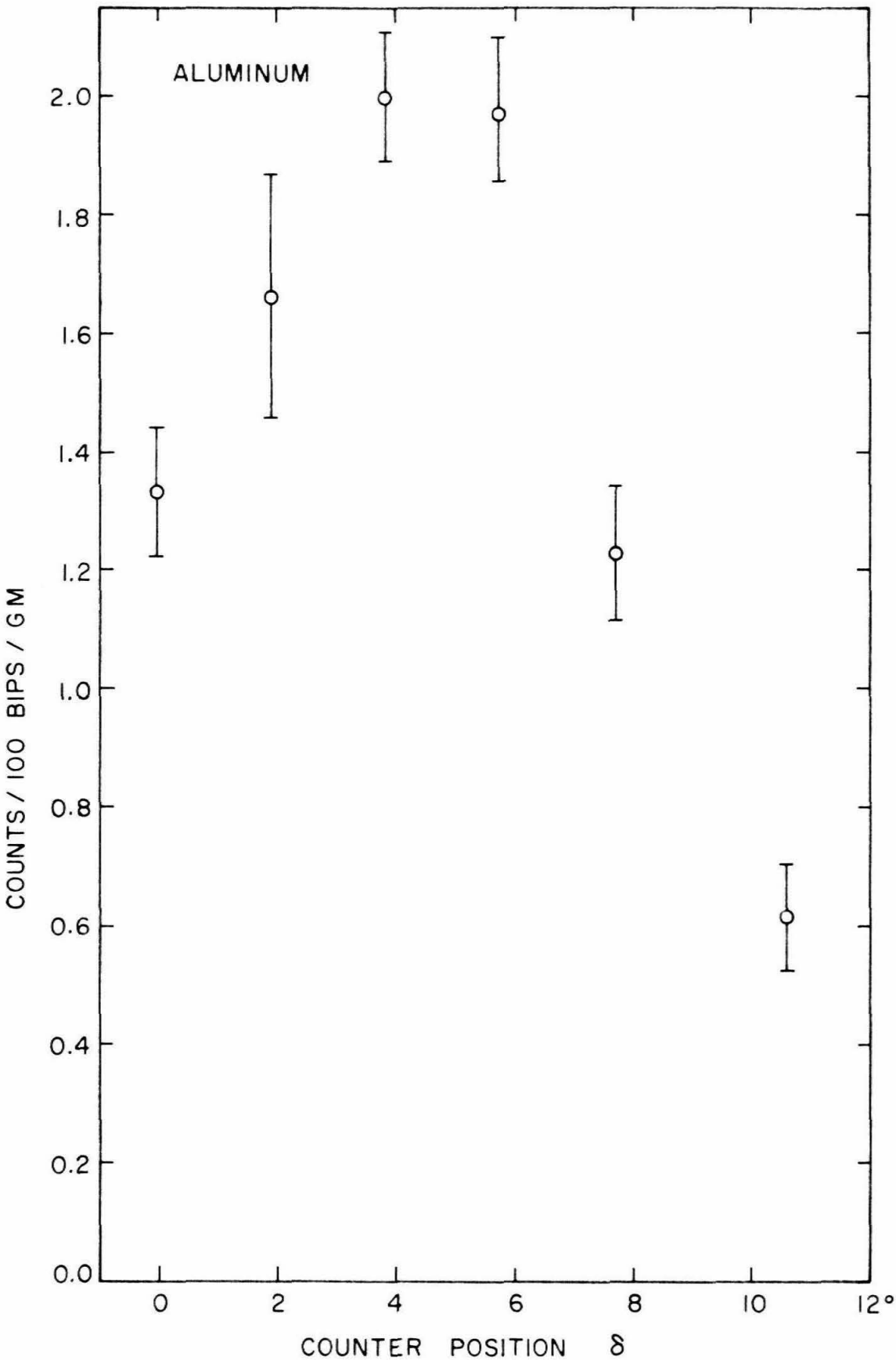
ALUMINUM
COUNTS / 100 BIPS / GM
2.0
1.8
1.6
1.4
1.2
1.0
0.8
0.6
0.4
0.2
0.0
0
2
4
6
8
10
12°
COUNTER POSITION δ

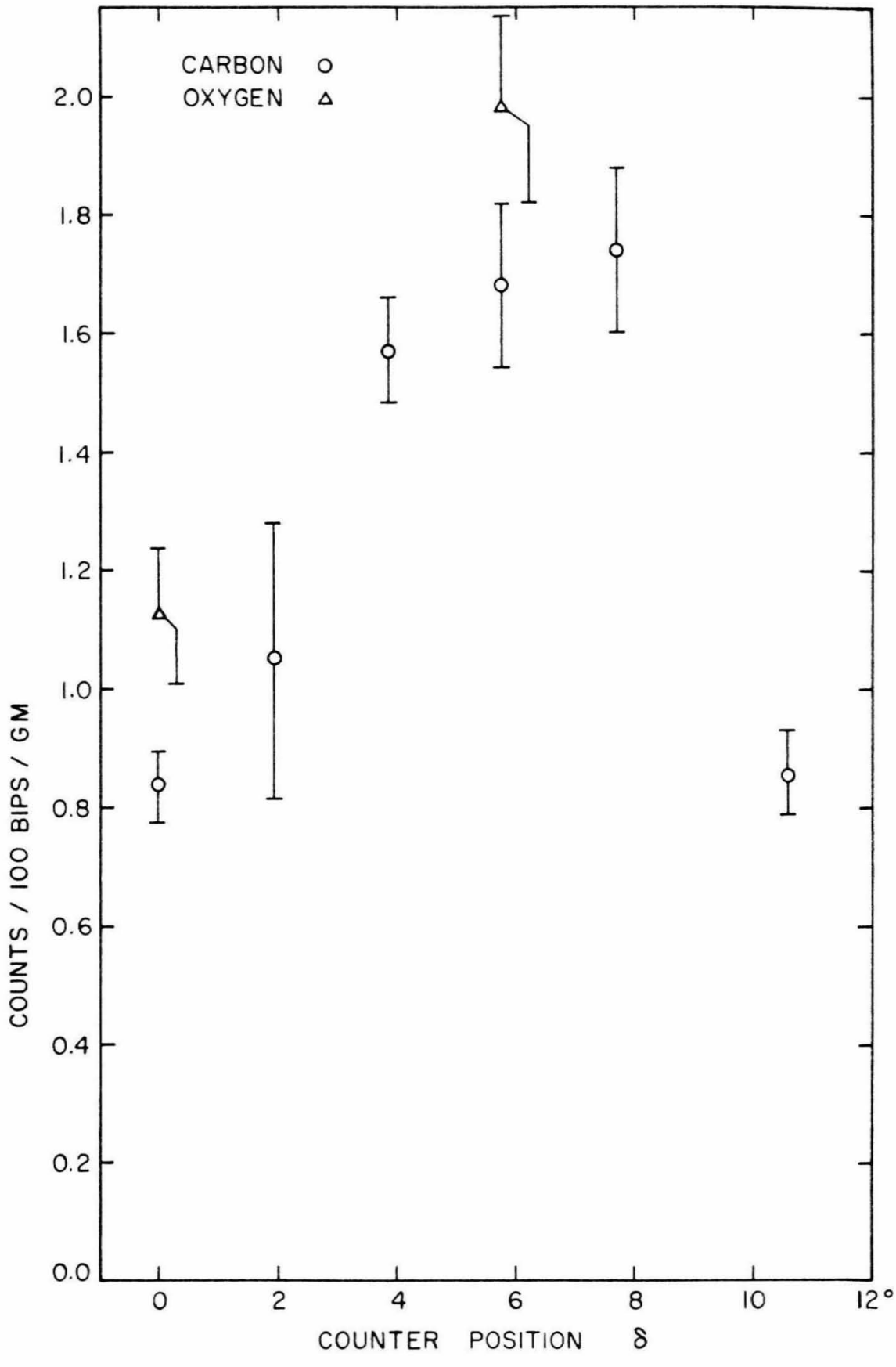
CARBON ○
OXYGEN △
2.0
1.8
1.6
1.4
1.2
1.0
0.8
0.6
0.4
0.2
0.0
COUNTS / 100 BIPS / GM
0
2
4
6
8
10
12°
COUNTER POSITION δ

Figures 14 - 17. A reconstruction of the differential cross section calculated by unfolding the counter resolution as described in the text. The statistical significance of the error flags is not correct as they have been overestimated. The vertical scale is approximately the cross section in $\mu b/sr$ divided by A. The solid and dashed curves on the left are the best fits for the lower and upper limits for the lifetime of 2×10^{-17} sec and 1.5×10^{-16} sec, respectively. The curves on the right labelled A, B and C are the calculated angular distributions for the π^o lifetime of 6×10^{-17} sec, the interference with a relative phase angle of 0^o, and the coherent nuclear with a non-spin flip cross section of $30 \sin^2\theta \, \mu b/sr$ in the center of mass corrected for absorption.

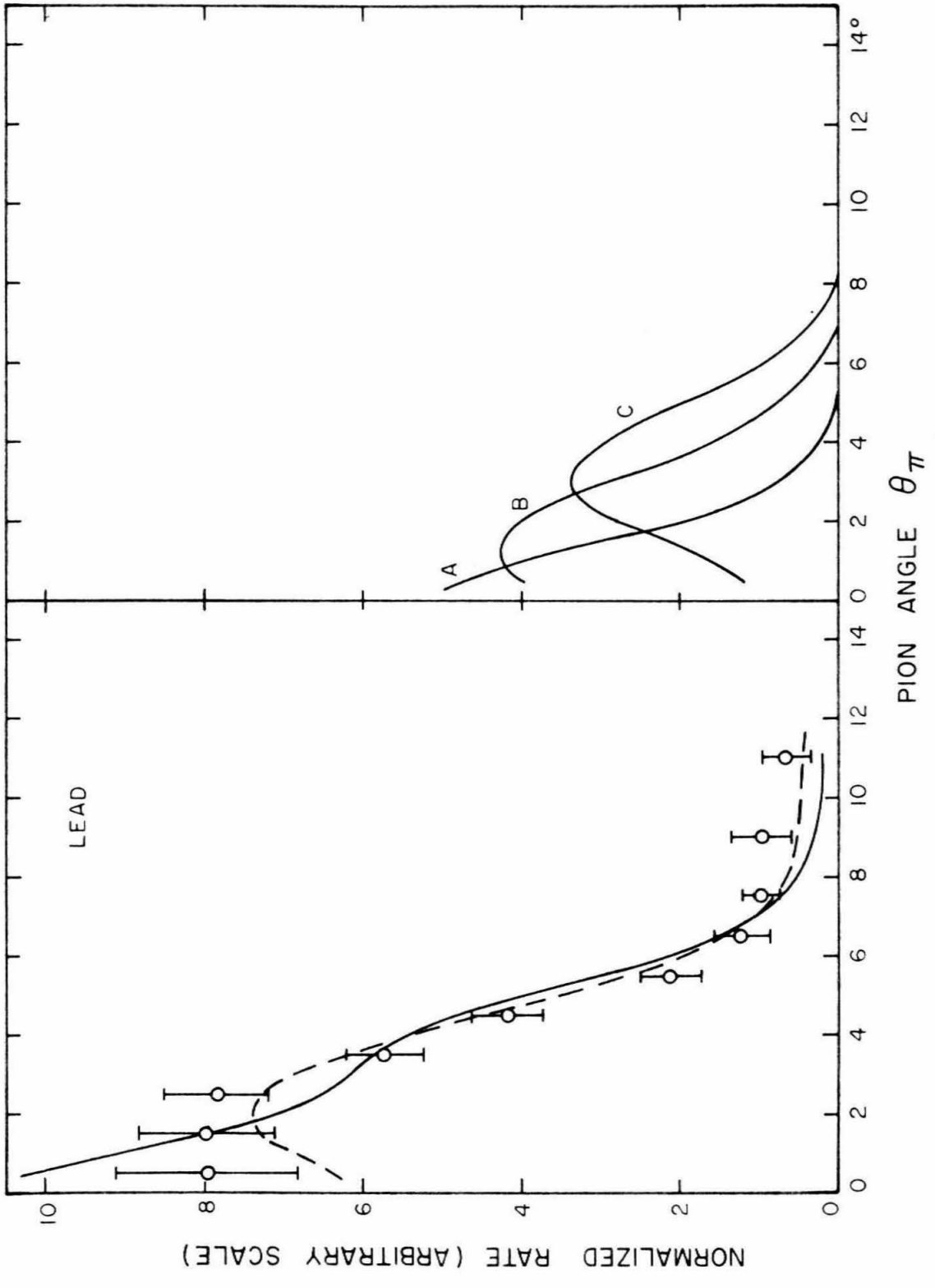
LEAD
A
B
C
NORMALIZED RATE (ARBITRARY SCALE)
PION ANGLE θ_π
0
2
4
6
8
10
12
14°

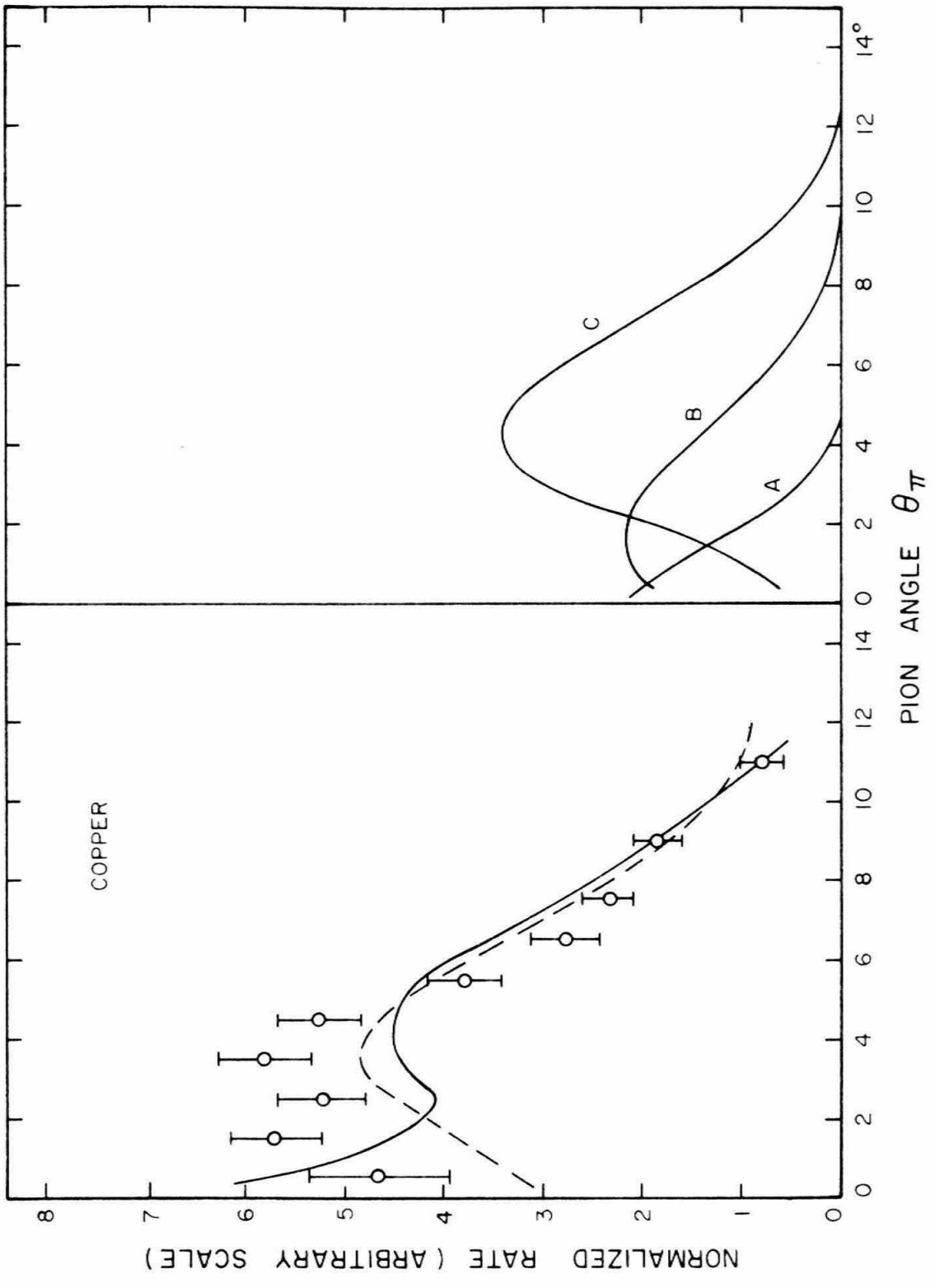
COPPER
A
B
C
NORMALIZED RATE (ARBITRARY SCALE)
PION ANGLE θ_π
0
2
4
6
8
10
12
14°

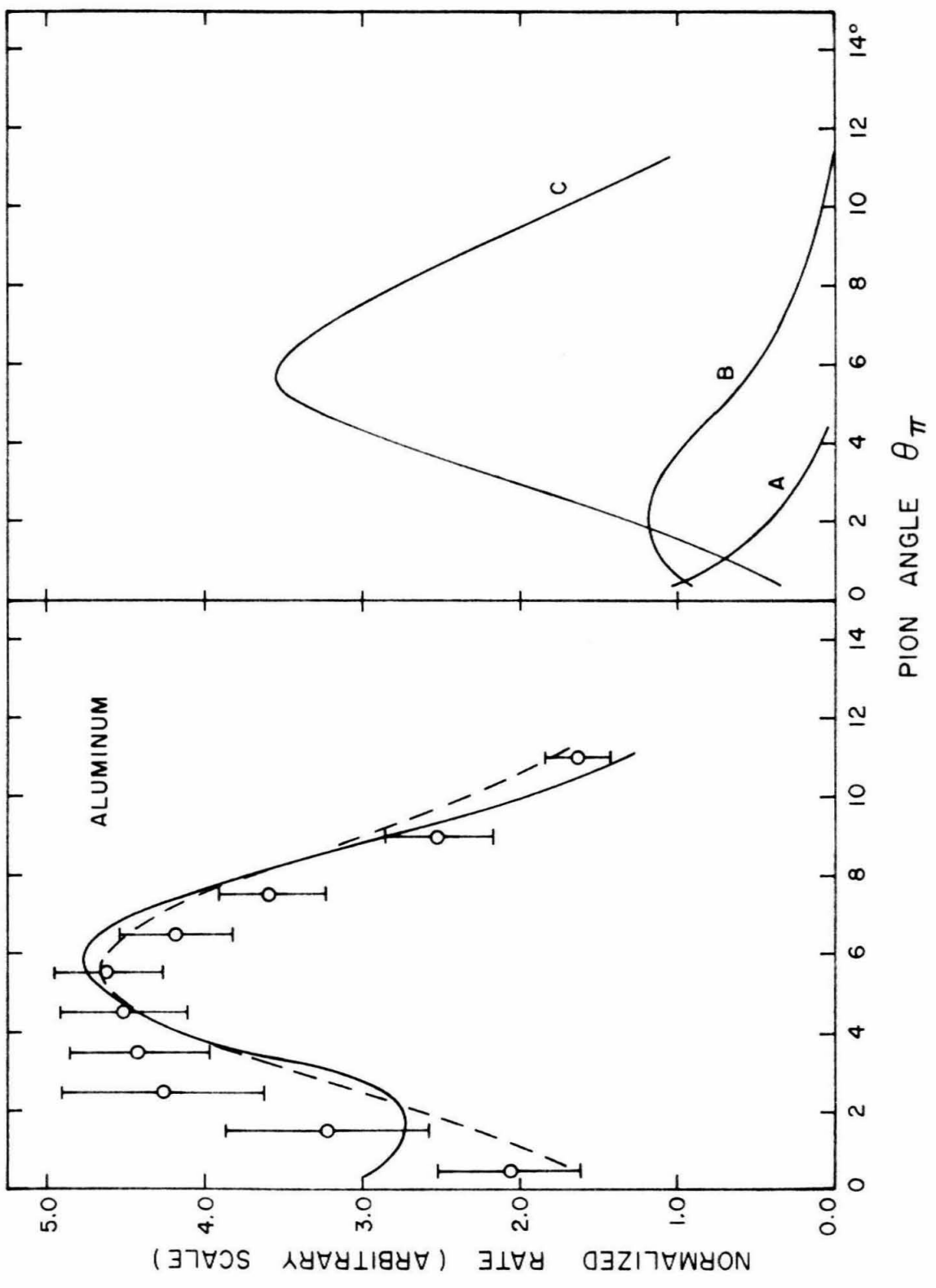
ALUMINUM
NORMALIZED RATE (ARBITRARY SCALE)
5.0
4.0
3.0
2.0
1.0
0.0
0
2
4
6
8
10
12
14
A
B
C
PION ANGLE θ_π

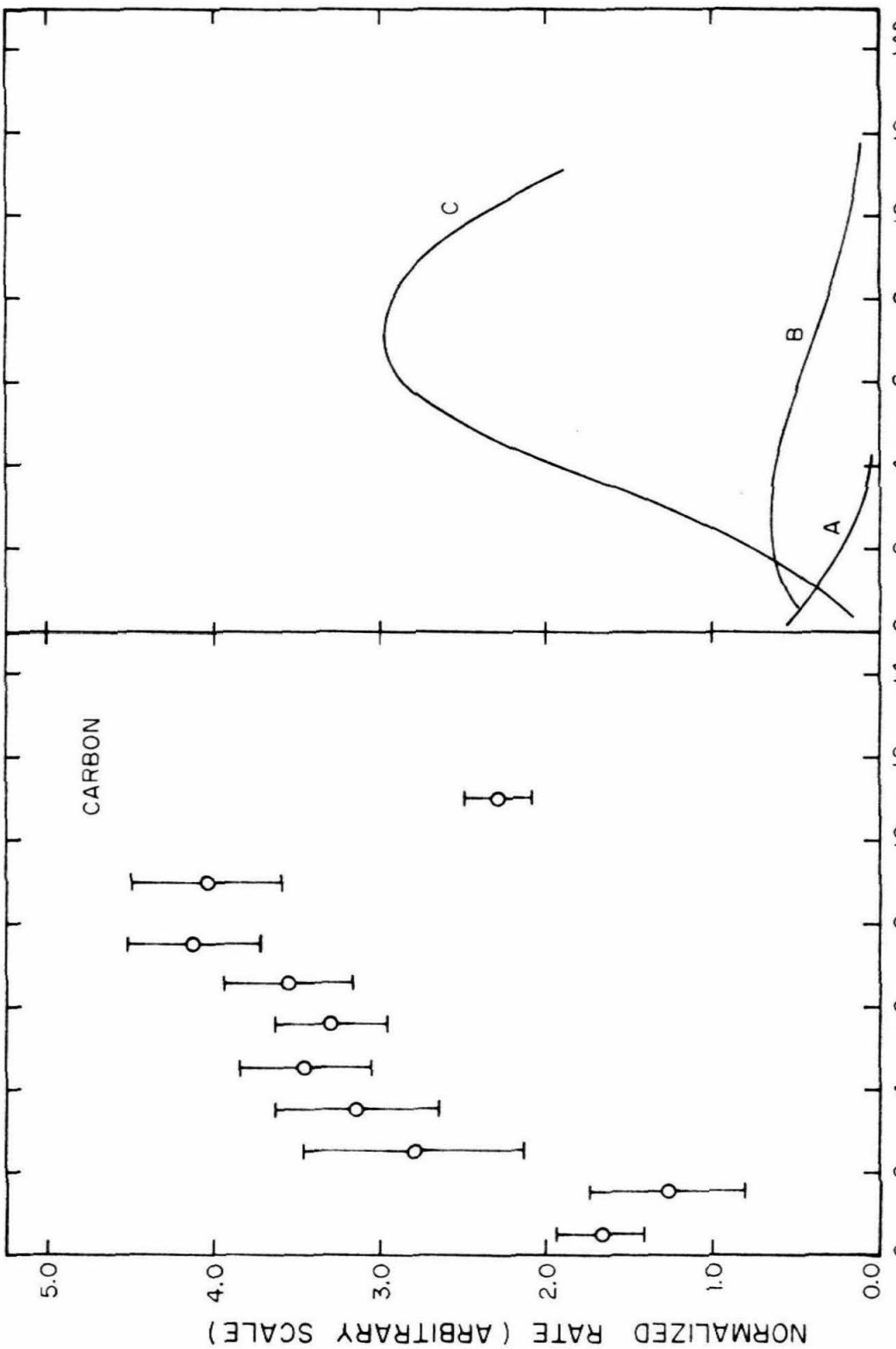
CARBON
A
B
C
NORMALIZED RATE (ARBITRARY SCALE)
PION ANGLE θ_π
0.0
1.0
2.0
3.0
4.0
5.0
0
2
4
6
8
10
12
14
14°

B. Backgrounds

Excluding showers produced in the target, there are three other sources of γ-rays in the true coincidence: 1) double Compton effect, 2) double π^o photoproduction in which one photon from each pion is detected, and 3) double pion photoproduction in which at least one of the pions is neutral and both photons come from its decay. The kinematics of the double Compton effect (10) are such that the photons that could be detected have energies of less than 100 Mev. For double π^o production in the energy range of interest the solid angle is an order of magnitude smaller for detecting γ-rays from different pions than for detecting them both from the same pion. The criterion on photon energy that the event be "pi like" will further reduce this contamination. The spectrum from this process would not show the characteristic π^o peak but should fall rapidly with energy. This may provide a contribution to the low energy events.

The pion pairs, then, where both photons come from a single π^o are the major source of background. If both pions are neutral, they could be produced coherently in the forward direction; however, this would involve momentum transfers of the order of the pion mass so that the form factors would be small. Thus the pion pairs are probably produced incoherently and would not have a rapidly changing angular distribution. An estimate of 0.3 counts/100 bips/gm for this counting rate has been calculated using a total cross section for charged pion pairs of 60 μbarn (11), assuming the momentum distribution given by phase space, and including a factor of three for the three possible neutral

pions produced (one from $\pi^{\pm} + \pi^{o}$ and two from $\pi^{o} + \pi^{o}$). A rate this large is comparable to the observed counting rates so that this effect has been included in attempts to fit the data.

To see if the calculation just outlined was reasonable, the counting rate from double pi zero production where one photon from each pion is detected has also been calculated using the same total cross section. The result showed the same energy dependence as the low energy background but was factor of 3-5 smaller. If this were much larger than the low energy background, we could rule out the contribution from the case in which both photons come from the same π^{o}, but this does not appear to be true.

The cosmic ray backgrounds from particles traversing both counters gave an equivalent counting rate on the order of 0.1 counts/100 bips; but because these events were cancelled out to within the counting statistics at each point when the target out rates were subtracted, they have been ignored.

C. Fitting of Data to Theoretical Counting Rates

The fitting of the measured angular distributions to the theoretical rates as calculated by a Monte-Carlo integral (see Appendix F) was done using a maximum likelihood technique (12). The parameters fitted are the amplitude for the Coulomb production (taken as real), the real and imaginary parts of the coherent nuclear amplitude, and the incoherent cross section. The amplitudes were chosen as parameters rather than the cross sections since they are a priori normally distributed. Since the

equations involved in the fitting procedure are non-linear, an iterative process was used to maximize the likelihood function.

The data have been fitted under two assumptions for the non-spin flip cross section, $(1/\sin^2\theta)d\sigma_{nsf}/d\Omega$. Since the angular range is small and the highest partial waves expected are $F_{5/2}$, the cross section can be taken as flat. However, since the recently discovered η particle of mass near 550 Mev (13) may have spin one, it may produce a pole in the photoproduction amplitude in the unphysical region at

$$\cos\theta = \frac{1}{\beta}\left(1 + \frac{m_\eta^2 - m_\pi^2}{2kE_\pi}\right)$$

in the center of mass. The contribution to the cross section from this term has been calculated and has been used in the fitting of the carbon and aluminum data. For small angles the cross section is

$$\frac{1}{\sin^2\theta}\ \frac{d\sigma_p}{d\Omega} = C\ \frac{p^4}{(q^2 + m_\eta^2)^2}\ . \qquad (10)$$

The factor C is related to the transition rate Γ for $\eta \rightarrow \pi^o + \gamma$:

$$C = 36\left(\frac{m_\eta}{m_\eta^2 - m_\pi^2}\right)^3\left(\frac{\gamma_{\eta NN}}{4\pi}\right)^2\Gamma\ , \qquad (11)$$

which can be further related to the π^o lifetime (14) :

$$C = 72\,\frac{(\gamma_{\eta NN}^2/4\pi)(\gamma_\eta^2/4\pi)}{\tau_{\pi o} m_\pi^3 \alpha} \qquad (12)$$

where α is the fine structure constant and $\gamma_{\eta NN}$ and γ_η are the re-normalized coupling constants defined in reference 14. A fit has not been

attempted using a pole due to an ω meson of mass 780 Mev since it would have little effect on the angular distribution in the range measured.

In addition to a cross section for the incoherent processes given by equation 7, the data have alternatively been fitted with a constant cross section to account for possible pion pair contamination.

Form factors of the form

$$F_{c,n}(q^2) = \exp\left[-\frac{1}{6}(qR_{c,n})^2 \right] \qquad (13)$$

where $R_{c,n}$ are the root-mean-square radii for the Coulomb and coherent nuclear processes were used in calculating cross sections and counting rates. Since absorption smooths out the minimum of the diffraction pattern and the exact shapes are not known, a better approximation for the form factors has not been used. For the same reason it has also been assumed that the phase of the interference term is independent of angle. The Coulomb form factors were calculated using the radii measured in the electron scattering experiments (15). A slightly larger radius was used in the coherent nuclear case which is consistent with pion absorption measurements (16) and with the low energy nuclear photoproduction data (2). The radii used in calculating the counting rates and the nuclear absorption of the coherently photoproduced pions as given by Engelbrecht (8) are summarized in Table II.

D. Discussion of Results

Table III summarizes the results of the fitting. For copper and lead, where the coherent production is more strongly peaked, the pole

TABLE II

Parameters of the target nuclei used in calculating cross sections for fitting to the data. The radii for the Coulomb and nuclear form factors, R_c and R_n, are in units of 10^{-13} cm. The column labelled C_a is the correction for nuclear absorption of the coherently produced pions from reference 8.

Target	R_c	R_n	C_a
Lead	5.42	6.68	4.75
Copper	3.67	4.51	3.25
Aluminum	2.7	3.40	2.60
Carbon	2.4	2.7	2.13

cross section was calculated from that without the pole by correcting for the factor $p^4/(q^2 + m_\eta^2)^2$ evaluated at 950 Mev and zero degrees. For the carbon data the angular range was not large enough to separate unambiguously the incoherent effects. The incoherent cross section was therefore set to zero (it actually fitted better slightly negative) which results in overestimating the coherent nuclear amplitude and giving a shorter value of the lifetime. A chi-square test of goodness of fit shows that only the lead and aluminum data without a pole have a reasonable fit. The errors on the fitting curves calculated by the Monte-Carlo integral, which would increase chi-square by 10-20%, had not been taken into account. The coherent nuclear cross section has been corrected for nuclear absorption of the pions using the factor C_a, which is the ratio of the cross section without absorption to that with absorption at the peak of the angular distribution as calculated with an optical model. The lifetime and non-spin flip results are not very sensitive to the choice of the incoherent cross section.

To give some idea of the angular dependence of the cross sections the best fits for lifetimes of 2×10^{-17} sec and 1.5×10^{-16} sec are plotted along with the data on the left halves of figures 14-17. To reiterate, the data in this method of presentation are not statistically correct but are only given to help visualize magnitudes and shapes. On the right sides of these figures the three curves labelled A, B, and C are the Coulomb, interference and coherent nuclear production counting rates, respectively, as calculated for a lifetime of 6×10^{-17} sec, a non-spin flip cross section of $30 \sin^2\theta$ μb/sr in the center of mass corrected for absorption, and a

Table III. A summary of the maximum likelihood fitting. The data have been fitted with the Coulomb and coherent nuclear amplitudes, their interference, and an incoherent cross section. For the non-spin flip nucleon cross section in cases C and D the angular distribution from a pole due to a mass 550 Mev particle was used. For carbon the incoherent cross section was constrained to be zero. The lifetime is given in units of 10^{-17} sec; cos ϕ gives the relative phase of the coherent nuclear amplitude; σ_{nsf} is the center of mass nucleon non-spin flip cross section in μb/sr which is corrected for absorption by the factor C_a in the next line; and the last lines are the laboratory incoherent cross section divided by A and the chi-square for the best fit.

TABLE III

	Lead	Copper	Aluminum	Carbon
Degrees of Freedom	19	11	11	5
A. Fit with constant incoherent and no pole				
lifetime	$10.4^{+3.1}_{-4.4}$	$3.1^{+1.2}_{-0.7}$	$7.5^{+3.2}_{-3.3}$	$1.68^{+0.58}_{-0.34}$
$\cos\phi$	1.00	-0.09	1.00	-0.18
$\sigma_{nsf}/\sin^2\theta$	6.43 ± 0.86	10.47 ± 1.56	13.16 ± 1.18	19.17 ± 1.4
xC_a	30.6 ± 4.1	34.1 ± 5.1	34.2 ± 3.1	44.1 ± 3.2
σ_i	0.51 ± 0.18	0.61 ± 0.19	0.08 ± 0.29	0
χ^2	24.2	30.7	11.4	20.1
B. Fit with correlated incoherent and no pole				
lifetime	$9.8^{+3.1}_{-4.5}$	$2.8^{+0.9}_{-0.6}$	$7.1^{+2.7}_{-2.8}$	
$\cos\phi$	0.97	-0.40	1.00	
$\sigma_{nsf}/\sin^2\theta$	7.01 ± 2.19	11.48 ± 1.37	13.24 ± 0.82	
xC_a	33.3 ±10.4	37.5 ± 4.5	34.4 ± 2.1	
σ_i	0.55 ± 0.20	0.48 ± 0.15	0.07 ± 0.21	
χ^2	23.3	30.9	11.4	
C. Fit with constant incoherent and with pole				
lifetime	a	a	$4.6^{+3.0}_{-1.3}$	1.0 ± 0.13
$\cos\phi$	a	a	0.035	-0.83
$\sigma_p/\sin^2\theta$	2.26 ± 0.30	4.03 ± 0.55	4.15 ± 0.47	7.57 ± 0.39
xC_a	10.8 ± 1.4	12.0 ± 1.8	10.8 ± 1.2	17.4 ± 0.9
σ_i	a	a	0.64 ± 0.29	0
χ^2	a	a	35.5	12.9

TABLE III (cont.)

	Lead	Copper	Aluminum	Carbon
D. Fit with correlated incoherent and with pole				
lifetime	a	a	$3.1\ ^{+0.8}_{-0.5}$	
$\cos\phi$	a	a	0.01	
$\sigma_p/\sin^2\theta$	2.46 ± 0.77	4.04 ± 0.48	4.85 ± 0.28	
xC_a	11.7 ± 3.7	13.2 ± 1.6	12.6 ± 0.7	
σ_i	a	a	0.23 ± 0.23	
χ^2	a	a	39.0	

(a) The entries in these positions are the same as the corresponding entries above since the pole term contribution has been calculated from the fit without a pole.

relative phase angle of 0^{o} between them. The ambiguity between the interference and lifetime effects is demonstrated for lead by the fact that a factor of two in the lifetime can be partially compensated by changing the phase angle by 80^{o}. A typical best fit is shown for lead in figure 18.

Since the theory of Engelbrecht of the incoherent production is supposed to be more exact for a closed shell nucleus, data were taken on oxygen, which is closed shell, to compare with the carbon data, which may show effects of the large magnetic dipole transition to a 15 Mev state. As can be seen from figure 13 there is no significant difference between the carbon and oxygen data. This effect may be masked by a contamination of pion pairs. The oxygen data was not further analyzed.

An attempt was made to discover how sensitive the results were to changes in the data and fitting parameters. A five per cent gain change in one of the Cerenkov counters would change the counting rate by two per cent. A ten per cent decrease in the carbon radius for nuclear production increased chi-square by seven making it a very much worse fit. In addition the best fit nuclear cross section changed by 15 per cent. Although it has a large effect on the goodness of fit, it was felt that leaving the radius to be a free parameter to be fitted would have made the procedure even more ambiguous.

Figure 18. The best fit curve for lead with the resolution unfolded is plotted with the data. The vertical scale is the same as in figures 14-17.

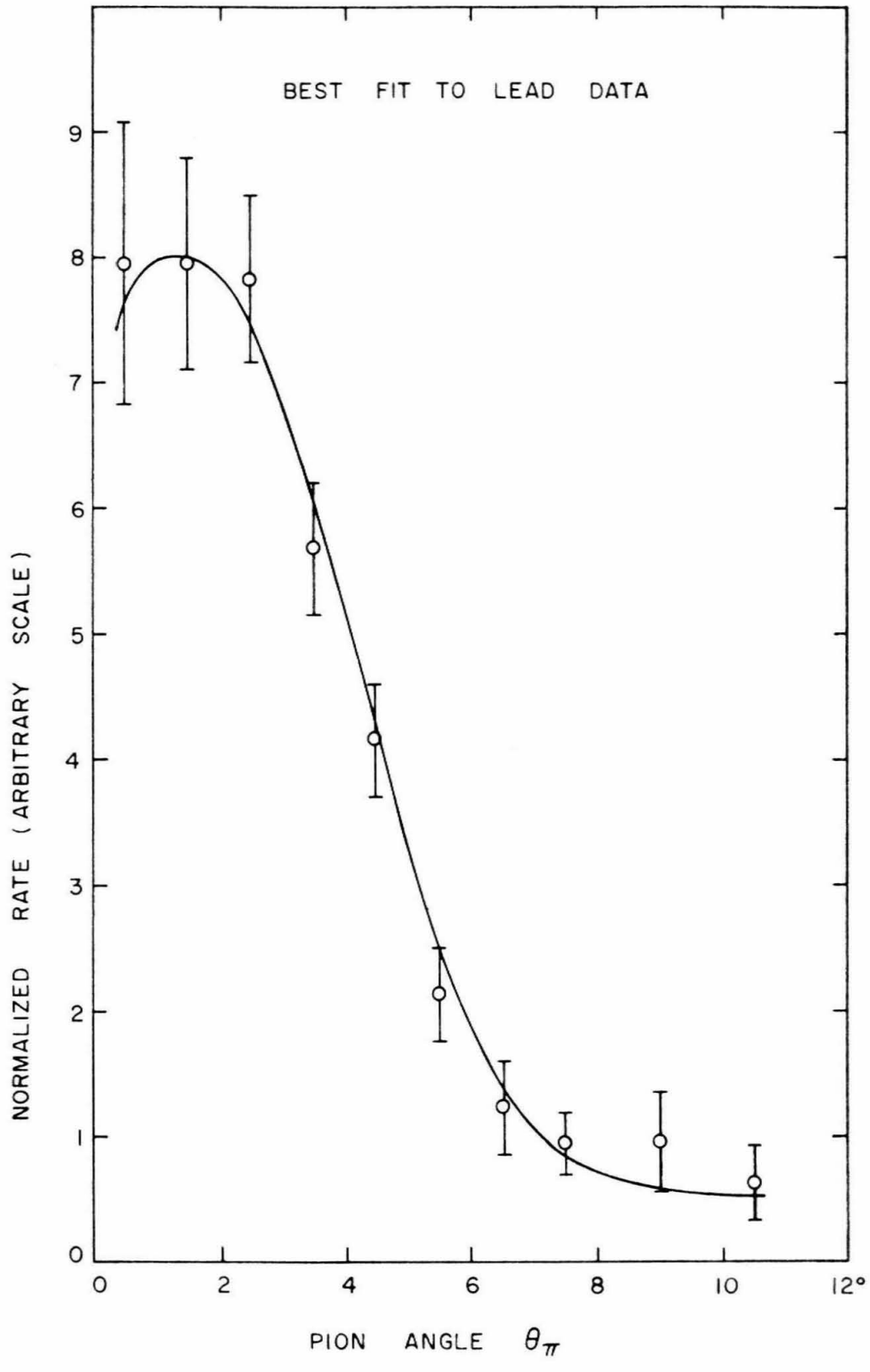
BEST FIT TO LEAD DATA
NORMALIZED RATE (ARBITRARY SCALE)
0
1
2
3
4
5
6
7
8
9
0
2
4
6
8
10
12°
PION ANGLE θ_π

V. CONCLUSIONS AND SUGGESTIONS

Although the data do not appear to be consistent there are several conclusions that can be drawn from them. The main contribution to the counting rate appears to come from the coherent nuclear production. There are, however, at angles smaller than the coherent peak, counts which can not be attributed to this process. If we assume that they come from the Coulomb and interference terms, we can put broad upper and lower limits on the lifetime. Any attempt to sharpen these limits runs into several difficulties: The angular resolution and the counting rates are not high enough to separate cleanly the Coulomb and interference terms; the uncertainties in the effects of absorption and the shape of the background make the fitting itself doubtful. Taking into account all the data except carbon, one can exclude lifetimes greater than 1.5×10^{-16} sec and shorter than 1×10^{-17} sec.

A stronger statement can be made about the neutral pion lifetime if we accept only the lead and aluminum data which gave a reasonable probability in a chi-square test. Combining these data and correcting by 8% for absorption gives a lifetime of $7.6 \, {}^{+4.2}_{-2.3} \times 10^{-17}$ sec. A plot of the likelihood function vs. lifetime is shown in figure 19. The errors quoted are for a 90% confidence level assuming they are purely statistical. Because of the possible systematic effects a more conservative estimate of the lifetime is $7.6 \, {}^{+6.0}_{-4.5} \times 10^{-17}$ sec.

Theoretical calculations which are based on perturbation theory (17) or on a dispersion theory calculation using only a limited number of

Figure 19. Likelihood curve for the π^0 lifetime from combining the lead and aluminum data assuming only statistical errors.

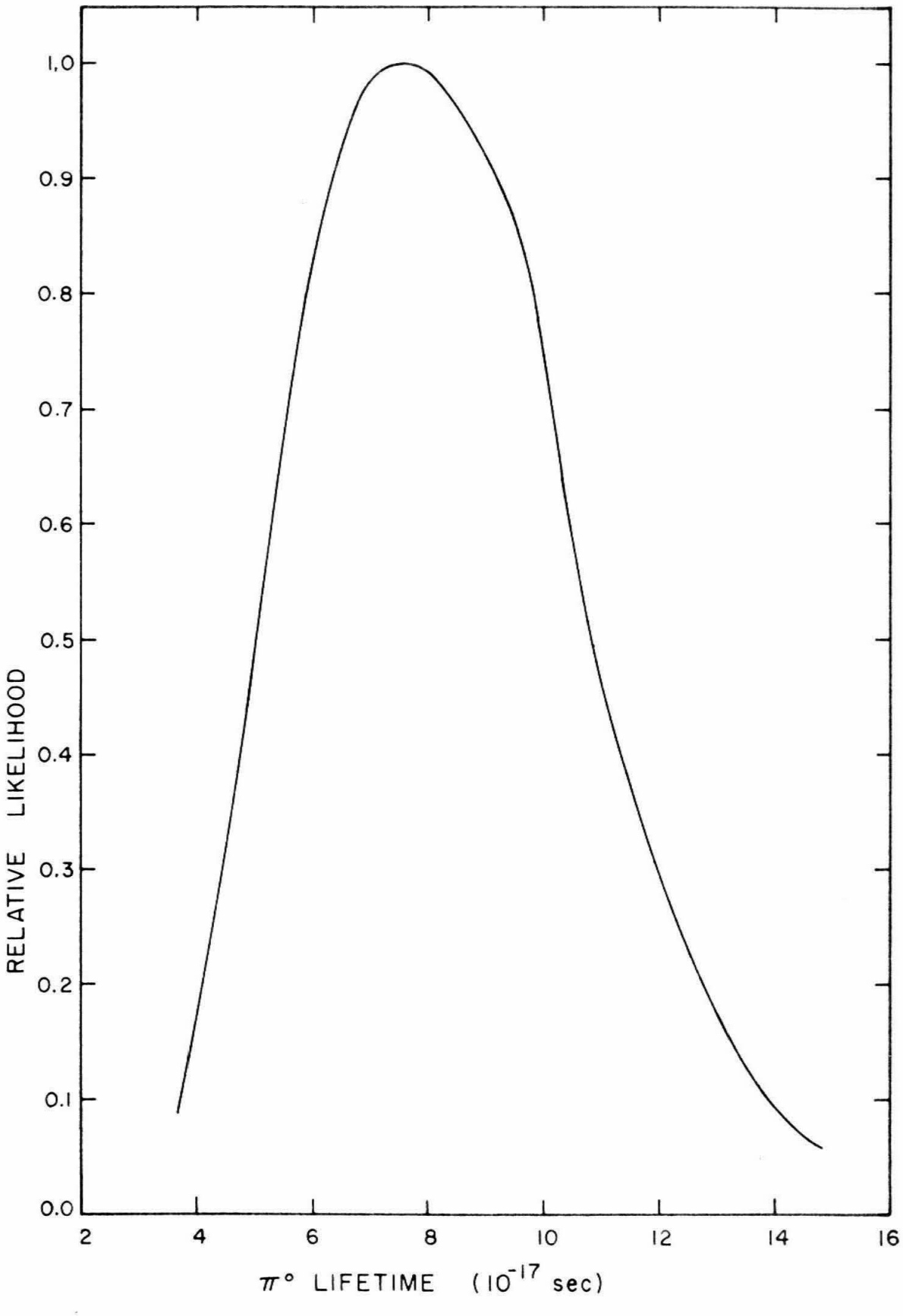
1.0
0.9
0.8
0.7
0.6
0.5
0.4
0.3
0.2
0.1
0.0
RELATIVE LIKELIHOOD
2
4
6
8
10
12
14
16
π° LIFETIME (10^-17 sec)

intermediate states (18) predict lifetimes in the range 5 - 20 x 10^{-17} sec. Mathews and Jacob (19), in their analysis of the contribution of the π^o pole to Compton scattering from protons, estimate from the data that the lifetime lies between 5 x 10^{-19} and 10^{-16} sec. This experiment can say nothing about the validity of these calculations.

The results of this experiment indicate a shorter lifetime than the more direct methods outlined in the introduction. The experiments involving the $K_{\pi 2}$ decay have recently been brought into question (20) in that there may be systematic errors or psychological biases in the measurement of events. These two types of experiments complement each other in that they can put lower and upper limits on the lifetime.

All the data, with the possible exception of carbon which is higher, when corrected for absorption, agree that the non-spin flip nucleon cross section at small angles goes like (33 ± 3) $\sin^2\theta$ μb/sr in the center of mass. This is much larger than would be expected from the published hydrogen data at a cm angle of 27.6° and 950 Mev (21), which would give about 5 $\sin^2\theta$ if it were all non-spin flip. Thus it appears that the non-spin flip cross section is peaked at small angles. This has recently been confirmed in the preliminary data of Talman et al. (22) measured with the same technique as in this experiment. If the forward peaking of the cross section is taken as an indication of a pole due to the exchange of a neutral vector meson, then since the cross section appears to be large for elements with nearly equal numbers of protons and neutrons, one can conclude that the vector meson is an isoscalar.

From the data in this experiment a determination of the mass of

the vector meson cannot be made except to note that for aluminum the fit to the data is very much worse if we assume a mass of 550 Mev. On the other hand, if the Gell-Mann and Zachariasen theory (14), which predicts a relationship between the vector meson and the π^o decay rates, is correct, then it is difficult to explain why the pole term is so large if it were due to an ω meson of mass 780 Mev. Taking a π^o lifetime of 10^{-16} sec and $\gamma_\omega^2/4\pi = 1/2$ (23) gives a width for the decay $\omega \rightarrow \pi^o + \gamma$ of 0.18 Mev. From the pole term with $\gamma_{\omega NN}^2/4\pi = 1/2$ (23) the width is 3.5 Mev. This discrepancy, however, may just be due to our poor knowledge of the coupling constants. For the η the decay widths are 0.22 Mev from the coherent nuclear cross section and 0.13 Mev using a lifetime of 10^{-16} sec and the same choice of coupling constants.

Although the absorption correction of Engelbrecht does give a consistent result for the non-spin flip nucleon cross section, the value of 33 $\sin^2\theta$ μb/sr is a factor of three larger than the preliminary results of Talman et al. from hydrogen. Thus the decay widths may be a factor of three smaller or there is a large difference between the neutron and proton non-spin flip cross sections. A measurement of the coherent production from deuterium would help in clearing up this point. The validity of the optical model at these energies is still in doubt.

The incoherent production when corrected for absorption is in rough agreement with the preliminary data of Talman et al. (22) at 940 Mev and 0^o. There is no evidence that the suppression due to the Pauli principle is stronger in a closed shell nucleus than in another.

The basic experimental difficulty with this method of measuring the π^o lifetime is the poor angular resolution. This resolution can be reduced to $\pm 1/2^o$ if the gamma rays are allowed to convert in spark chambers set in front of the Cerenkov counters. The energy resolution should not be greatly affected, but the counting rate would be reduced. The energy acceptance of the telescopes should also be reduced to eliminate background events from neutral pions produced in pairs. Both of these improvements require a more intense photon beam.

Since the contribution from the Coulomb process increases with energy while the coherent nuclear should be reduced because the form factor decreases, the experiment would appear to be cleaner at higher photon energies. However, if the nuclear production is dominated at small angles by a vector meson intermediate state, then it would increase roughly at the same rate as the lifetime and the improvement would be small. Thus it may turn out that the indirect method for measuring the π^o lifetime is unsatisfactory and that high energy nuclear stars will give the most accurate value.

APPENDICES

A. Synchrotron Beam

The 1.2 Gev circulating electron beam inside the synchrotron is allowed to spill out over a period of 50 msec onto a 0.2 radiation length tantalum target. The gamma ray beam emerges from the machine through a 1/4" x 3/8" primary collimator and then through the first scraping wall. Immediately behind the first scraper is a small sweeping magnet to deflect charged particles from hitting the target for this experiment. The beam, after passing through the target and being swept again, goes between the two counter systems in a helium filled tube, then through the second scraper and a liquid hydrogen target if the latter is in the lowered position. The beam is finally stopped in a thick wall ionization chamber.

The beam intensity was normally monitored by this thick walled chamber (called chamber III) which was made of copper and contained an argon-CO_2 mixture. A second "thin" chamber located between the primary collimator and the first scraper and consisting of two parallel plates that collected ions produced by the beam passing between them was used for monitoring when the high energy magnet was at small angles and intercepting the beam before it could reach chamber III. At these times the thin chamber was calibrated against chamber III. The current from the chambers was integrated and recorded in units called bips (beam integrator pulses). From the integrator constant and the chamber calibration one has the beam intensity integrated over energy.

During the course of this experiment chamber III was calibrated

several times by Gomez against a Wilson type Quantameter (24) whose response as calculated from shower theory is independent of the spectrum. The results of these calibrations differed from one another by about 2 per cent when corrected for a slow drift due to leakage from the chamber. This discrepancy is outside of experimental error and has not been explained. An average value of 4.15×10^{18} Mev/coulomb for an end point energy of 1200 Mev has been used in analyzing the data. The integrator calibration measured frequently during the experiment was 0.211 μcoulomb/bip with a fluctuation of less than one half per cent. The over all calibration is then 0.877×10^{12} Mev/bip.

B. Apparatus

A plan view of the experimental arrangement is shown in figure 6. A 1.2 Gev bremsstrahlung beam from the synchrotron was incident on the target supported between the pole pieces of a sweeping magnet. The beam in the region between the target and the detector system was enclosed in a helium filled mylar bag to reduce background. At the target the beam filled an area of approximately one inch square, but was strongly concentrated at the center. The lateral spread of the beam has been ignored in the analysis of the data.

Both of the decay gamma rays from the neutral pions produced in the target were detected in total absorption spectrometers. These Cerenkov counters consisting of $14'' \times 14'' \times 12''$ blocks of lead glass had a linear energy response and a resolution of 6.1 per cent at one Gev (25).

The angular resolution of the counter was defined by a 6.1" x 3.1" aperture in 4" thick lead walls 89.25" from the target. The centers of the apertures were chosen to be $8^{\circ}40'$ on either side of the beam, since this is the symmetric decay angle for a π^{o} with a total energy of 900 Mev.

The charged particle background was eliminated by sweeping them in the vertical direction and by 4" x 7" veto counters in front of the apertures. A 1.5" piece of paraffin removed the extremely low energy particles. The background due to cosmic ray particles traversing both Cerenkov counters was reduced by the cosmic ray veto counters located between the two Cerenkovs just to the left of the beam. These were shielded both from the beam and from the nearby Cerenkov.

The counter cells sit on a large table which can move both counters simultaneously in the vertical direction. By this procedure an "angular distribution" of the pions can be measured. The shielding and anti-coincidence counters are mounted so that they move as a unit with the Cerenkovs.

The physical properties of the targets are summarized in Table IV. The liquid oxygen was contained in a small vacuum flask taken from a thermos bottle.

C. Electronics

A block diagram of the fast electronics is shown in figure 7. The primary identification of a pion is done by a ten nanosecond coincidence between pulses from the two Cerenkov counters, A(456) and B(456).

TABLE IV

Target Properties

Material	Z	A	gm/cm^2	Absorption
Lead	82	207.2	0.582	0.07
Copper	29	63.57	1.43	0.06
Copper	29	63.57	2.94	0.13
Aluminum	13	26.97	3.09	0.10
Carbon	6	12.00	4.32	0.075
Oxygen	8	16.00	7.98	0.155 (net)

The output of this coincidence, AB(456), opens a 50 nsec linear gate which passes the A and B signals from the Cerenkov counters. There is an additional output from the gate for the sum signal A + B. The pulses from the veto counters, 1A and 1B, are first required to be in 25 nsec coincidence with the A(456) and B(456) signals from the corresponding Cerenkov counter before being sent to the slow logic to decrease the veto dead time. The signals from the cosmic ray veto counters are added to the 1A signal before the fast coincidence.

The slow electronics shown in figure 8 does the final biasing and logic to define the event as a π^o and records the data for further analysis. The slow discrimination and logic is done in six channel discriminator and coincidence-anticoincidence circuit (Keck Box) with a coincidence resolving time of 0.3 μsec and a veto dead time of 0.7 μsec which is gated on during the beam dump. This circuit gives out a trigger when the gated signals from the two Cerenkov counters, A_g and B_g, are above a preset bias level, and the fast coincidence circuit has given a standard size pulse AB(456), and also there are no (1A· A) and (1B· B) pulses from the veto counters. The trigger turns on a twenty channel pulse height analyser (kicksorter) which records the pulse height of the A + B sum signal.

In addition, the individual gated counter pulses, A_g and B_g, are lengthened in the double gated stretcher and are applied to the horizontal and vertical deflection plates respectively of an oscilloscope. At the same time an unblanking signal is applied to the grid of the cathode ray tube to turn on the electron beam. This puts a dot on the screen

whose coordinates are proportional to the size of the original pulses out of the Cerenkov counters. The "dot plot" is photographed onto Polaroid-Land transparency film, which is developed after each run and filed for further analysis. The numbers of counts of the types $(1B \cdot B)$, B_g, $(1B \cdot B) \cdot B_g$, $(1A \cdot A)$, A_g, $(1A \cdot A) \cdot A_g \cdot AB(456)$, and the number of triggers are recorded on scalers.

D. Calibration Procedure

The standard energy calibrations of the Cerenkov counters are runs on cosmic ray muons traversing the counter vertically. The peak of the spectrum comes at an equivalent gamma ray energy of 201 Mev. This agrees well with the path length of the muons through the glass. The cosmic ray spectrum and that for 955 Mev electrons are shown in figure 20.

Before each day's running the output of a pulser is fed into the calibration inputs to the mixers of both Cerenkov counters. The gains of the electronics are adjusted to standard values and the biases of the fast coincidence circuits are checked. Day to day gain drifts are about 1 - 2 per cent. With the sweep magnet turned off electron calibrations are made to check drifts in the Cerenkov counters and to check the veto counters. This gives a sensitive measurement of the energy calibration because the electron spectrum falls sharply with energy.

The dot plots recording the correlated pulse heights for each event are calibrated against the kicksorter before each run. The output of a pulser is introduced into the system at the stretchers for first

Figure 20. Cerenkov counter response to cosmic ray muons and to mono-energetic electrons. The electron spectrum has been fitted to a Gaussian distribution with a width of 6.5 per cent.

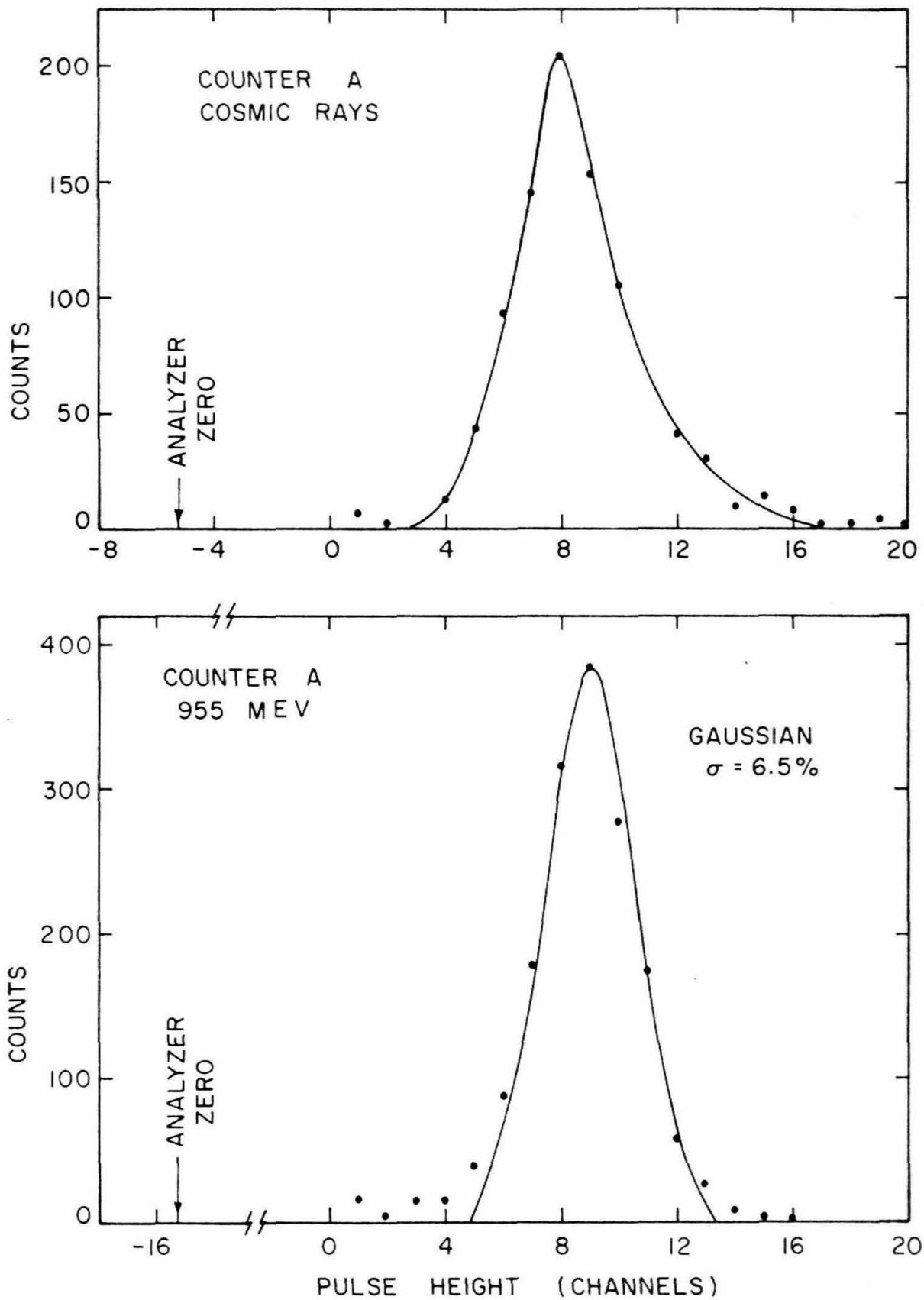
COUNTER A
COSMIC RAYS
COUNTS
ANALYZER ZERO
200
150
100
50
0
-8
-4
0
4
8
12
16
20
COUNTER A
955 MEV
GAUSSIAN
σ = 6.5%
COUNTS
ANALYZER ZERO
400
300
200
100
0
-16
0
4
8
12
16
20
PULSE HEIGHT (CHANNELS)

the A and then B side and the pulse height is adjusted to lie between selected channels of the analyzer. A series of these dots form the coordinate axes on the film. The oscilloscope position and gain are adjusted so that the dots fall at predetermined points in respect to the graticle.

E. Data Handling

The dot plots of pulse height in the two Cerenkov counters which are recorded on Polaroid transparency film are read by projecting the photograph on a rectangular graticle. With the calibration dots at a standard position the coordinates of the individual events are recorded in a notebook. The coordinates are also punched on IBM cards for analysis by an IBM 7090 computer.

The computer analysis is carried out in two steps. For each run a parameter card is read which contains the target material and thickness, counter position, beam end point and calibration, and the energy calibration of the individual counters. Also on the parameter card is the number of bips and triggers that occurred during the run and the duration of the run in minutes. The coordinates of the events are then read and the kicksorter channel and photon energy are calculated. The spectrum of pulse heights corresponding to that recorded for the sum pulses on the kicksorter are printed out for comparison with the notebook. Agreement to one channel is required or the dot plot is reread.

From the energy of the γ-rays in the two counters and the geometry of the counter apertures the program calculates the maximum and minimum possible angles that the pion could be emitted to give the

measured split in energy. An event is defined as "π-like" if the difference between the maximum and minimum pion angle is positive. These events are flagged on the printout. The angles and energies calculated are stored in binary form on magnetic tape for further analysis.

The second analysis program reads the data that have been stored on tape into the computer. For a given set of runs the program selects events satisfying angle and energy criteria. Counting rates are calculated and histograms of energy distributions and pion angles are printed. The pion angle is defined in equation 9. The output of this program is the results used in interpreting the data.

F. Monte-Carlo Integral

The counting rate for neutral pions photoproduced from a complex nucleus is given by the five-dimensional integral

$$C_r = \frac{N_o t}{A} \int_0^{E_o} N(k)\, dk \int_0^{2\pi} d\phi_\pi \int_{-1}^{1} d\cos\theta_\pi \sigma(k, \theta_\pi) P(k, \theta_\pi, \phi_\pi) .$$

$N_o t/A$ is the number of target nuclei of mass number A in a target of thickness t.

$N(k) = \frac{W}{E_o} B(k, E_o)/k$ is the shape of the bremsstrahlung spectrum. W is the total energy in the beam per bip, E_o is the end point energy and $B(k, E_o)$ is the deviation from the $1/k$ distribution (26).

$\sigma(k, \theta_\pi)$ is the cross section for producing pions at angle θ_π by a photon of energy k.

$$P(k, \theta_\pi, \phi_\pi) = \frac{1}{4\pi} \int_0^{2\pi} d\phi_1 \int_{-1}^{1} d\cos\theta_1 \epsilon(k, \theta_\pi, \phi_\pi, \theta_1, \phi_1)$$

is the probability of detecting a π^o of total energy k and angles θ_π, ϕ_π. θ_1 and ϕ_1 are the center of mass directions of one of the decay γ-rays and

$$\epsilon = \begin{cases} 1 \text{ if both } \gamma\text{-rays are detected} \\ 0 \text{ otherwise} \end{cases}$$

The integral has been programmed for an IBM 7090 computer using a Monte-Carlo technique.

The Monte-Carlo integral may be best illustrated by a simple example in one dimension. Suppose we wished to compute $\int_0^1 y(x)\, dx$ where the integrand is normalized such that $0 < y < 1$. We would choose a set of N uniformly distributed random numbers $0 \leq x_n \leq 1$ and compute $y(x_n)$. These are compared with a second set of similarly distributed random numbers $0 \leq y_n \leq 1$. The ratio of the number of times $y(x_n) \geq y_n$ to the total number of trials N will approach the true value of the integral as N becomes larger. This technique is useful in evaluating the counting rate integral because we are able to duplicate the physics of the problem and get intermediate results such as angle and energy distributions.

The integration program is divided into two parts. The first part generates events that can be detected by the counter system and stores the pion angle and energy on magnetic tape. The second program does the actual integration by folding together the cross section, bremsstrah-

lung spectrum, and counter energy resolution. The functional dependence of the cross section can be easily specified and bias conditions on angles and energies similar to those in the analysis programs can be imposed.

The generating program chooses randomly the five independent parameters k, θ_π, ϕ_π, θ_l, ϕ_l. A Lorentz transformation into the laboratory system along the pion direction is performed on the γ-rays to see if they have both been detected. If they both are, then their laboratory energies are calculated and the parameters of the event are stored on tape. The expected counting rates have been calculated using 2000 events generated by this program for each counter setting.

The integration program reads in the event parameters from tape and calculates the cross section and bremsstrahlung spectrum. To fold in the energy resolution of the counters two new photon energies distributed normally about the energies recorded on tape with a width given by $\sigma = 61\sqrt{E}$ Mev, where E is the incident photon energy in Gev, are calculated. The events are then handled exactly as in the data analysis programs to see if it passes the angle and energy criteria. The pion angle is calculated as described above, and histograms are made of angle and energy distributions.

For each event on tape five folded events are used to smooth out the distributions. The counting rate itself is calculated by summing the integrands and dividing by the proper normalization factor. An "experimental" value of the error on the integral is gotten by dividing the 2000 events into ten groups and finding the spread in the distribution of counting rates. The overall errors on the counting rates are about 3 per cent.

REFERENCES

1. H. Primakoff, Phys. Rev. 81, 899 (1951).

2. G. Davidson, Ph. D. Thesis, Massachusetts Institute of Technology (1959).

3. Blackie, Engler, and Mulvey, Phys. Rev. Lett. 5, 384 (1960).

4. Glasser, Seeman, and Stiller, Phys. Rev. 123, 1014 (1961).

5. Shwe, Smith, and Barkas, private communication; see also Phys. Rev. 125, 1024 (1962).

6. S. M. Berman, private communication; see also Glaser and Ferrel, Phys. Rev. 121, 886 (1961).

7. S. M. Berman, Nuovo Cimento 12, 1020 (1961).

8. C. A. Engelbrecht, Ph. D. Thesis, California Institute of Technology (1961).

9. H. Primakoff, Rev. Mod. Phys. 31, 802 (1959).

10. Jausch and Rohrlich, "Theory of Photons and Electrons," Addison-Wesley (1955).

11. Chasan, Cocconi, Cocconi, Schechtman, and White, Phys. Rev. 119, 811 (1960).

12. J. Orear, "Notes on Statistics for Physicists," UCRL-8417

13. Pevsner et al., Phys. Rev. Lett. 7, 421 (1961).

14. Gell-Mann and Zachariasen, Phys. Rev. 124, 953 (1961) (Note that there is an error of a factor of four in equation 5.12 of this paper)

15. R. Hofstadter, Ann. Rev. Nucl. Sci. 7, 231 (1957).

16. L. R. B. Elton, Rev. Mod. Phys. 30, 557 (1958).

17. R. J. Finkelstein, Phys. Rev. 72, 415 (1947); J. Steinberger, Phys. Rev. 76, 1180 (1949).

18. Goldberger and Trieman, Nuovo Cimento 9, 451 (1958); How-sen Wong, Phys. Rev. 121, 289 (1961).

19. Jacob and Mathews, Phys. Rev. 117, 854 (1960).

20. Discussion with G. Quarini.

21. Berkelman and Waggoner, Phys. Rev. 117, 1364 (1960).

22. Talman, Clinesmith, Gomez, and Tollestrup, private communication (to be published in Bull. Am. Phys. Soc.).

23. Gell-Mann, Sharp, and Wagner, Phys. Rev. Lett. 8, 261 (1962).

24. R. R. Wilson, Nucl. Inst. 1, 101 (1957).

25. Ruderman, Gomez, and Tollestrup, CTSL-31 (unpublished).

26. J. H. Boyden, Ph. D. Thesis, California Institute of Technology (1961).